VYSOKÉ UČENÍ TECHNICKÉ V BRNĚ
BRNO UNIVERSITY OF TECHNOLOGY

FAKULTA ELEKTROTECHNIKY A KOMUNIKAČNÍCH TECHNOLOGIÍ
FACULTY OF ELECTRICAL ENGINEERING AND COMMUNICATION

ÚSTAV BIOMEDICÍNSKÉHO INŽENÝRSTVÍ
DEPARTMENT OF BIOMEDICAL ENGINEERING

3D TISK KERAMICKÝCH KOSTNÍCH NÁHRAD S ROZDÍLNOU VNITŘNÍ STAVBOU
3D PRINTING OF CERAMIC BONE GRAFTS WITH DIFFERENT INTERNAL ARCHITECTURE

BAKALÁŘSKÁ PRÁCE
BACHELOR'S THESIS

AUTOR PRÁCE — **Ing. Lenka Novotná, Ph.D.**
AUTHOR

VEDOUCÍ PRÁCE — **prof. Ing. Ivo Provazník, Ph.D.**
SUPERVISOR

BRNO 2017

VYSOKÉ UČENÍ TECHNICKÉ V BRNĚ
FAKULTA ELEKTROTECHNIKY A KOMUNIKAČNÍCH TECHNOLOGIÍ

Bakalářská práce

bakalářský studijní obor **Biomedicínská technika a bioinformatika**
Ústav biomedicínského inženýrství

Studentka: Ing. Lenka Novotná, Ph.D. ***ID:*** 77217
Ročník: 3 ***Akademický rok:*** 2016/17

NÁZEV TÉMATU:

3D tisk keramických kostních náhrad s rozdílnou vnitřní stavbou

POKYNY PRO VYPRACOVÁNÍ:

1) Proveďte literární rešerši kostních náhrad a definujte klíčové chemicko-fyzikální vlastnosti (struktura, porozita, apod.) pro biomedicínské aplikace. Popište způsoby přípravy náhrad, zejména 3D tiskem, klady a zápory jednotlivých metod. 2) Proveďte obrazovou analýzu mikroskopických obrazů vybraných preparátů kostní tkáně a definujte jejich makro/mikrostrukturu. 3) Ve vhodném programovém rozhraní vytvořte 3D modely porézních nosičů s odlišnou vnitřní strukturou (tvar pórů, jejich velikost a distribuce). 4) Pomocí 3D tisku experimentálně připravte vybraná keramická porézní tělesa. 5) Výsledné produkty popište z pohledu výhod a nevýhod a výsledky diskutujte.

DOPORUČENÁ LITERATURA:

[1] GARIBOLDI, M.I. a BEST, S.M.: Effect of Ceramic Scaffold Architectural Parameters on Biological Response, Frontiers in Bioengineering and Biotechnology, 3 (2015).

[2] WNEK, G.E., BOWLIN, G.L.: Encyclopedia of Biomaterials and Biomedical Engineering, 2. vyd. Informa Healthcare, 2008. 3552 s. ISBN 142007802X.

Termín zadání: 6.2.2017 ***Termín odevzdání:*** 19.5.2017

Vedoucí práce: prof. Ing. Ivo Provazník, Ph.D.
Konzultant: Ing. Josef Jaroš, Ph.D., doc. Ing. Jana Kolářová, Ph.D.

prof. Ing. Ivo Provazník, Ph.D.
předseda oborové rady

ABSTRACT

Bioceramics in the form of scaffolds hold great promise in bone tissue regeneration. While the scaffold composition is important for biocompatibility, the internal architecture plays a key role in allowing proper cell penetration, nutrient diffusion, bone ingrowth, vascularization as well as mechanical properties. A solid freeform fabrication is a promising processing technique, allowing to study structural parameters independently.

This bachelor thesis is focused on ceramic bone replacements with different internal structure. The thesis is divided into 8 chapters. The first four chapters briefly summarize the current state of the art in the following fields: bone structure, requirements for synthetic bone replacements, scaffold architecture, and fabrication methods with an emphasis on 3D printing. The next chapters deal with experimental part. The image analysis of mouse skeleton was performed. On the basis of the measured pore size (50 – 200 μm) and according to the literature search, 16 structures with various shape, curvature and pore size were designed. The CAD models were printed by a stereolithography from a tricalcium phosphate dispersion. Sintered ceramic scaffolds exhibited an ideal structure for application in bone tissue engineering. Scaffolds contained both interconnected macro- and micropores of optimal sizes up to 500 μm and about 3 μm, respectively. The results confirm that stereolithography is suitable, and compared to others, precise method for preparing scaffolds having different internal structures. The individual structural characteristics influencing the scaffold behaviour will be possible to study independently to each other. And thus improve the scientific knowledge in the field of treatment of large segmental bone defects.

ABSTRAKT

Porézní biokeramické materiály se jeví být slibné jako dočasné kostní náhrady pro regeneraci kostní tkáně. Zatímco chemické složení ovlivňuje biokompatibilitu, vnitřní struktura je klíčová pro penetraci buněk, difuzi živin, vaskularizaci, vrůstání kosti; a zásadně ovlivňuje mechanické vlastnosti implantátu. Trojrozměrný tisk umožňuje připravit téměř libovolné struktury a nezávisle tak studovat jejich vliv.

Zadáním bakalářské práce bylo prostudovat a 3D tiskem připravit keramické kostní náhrady s rozdílnou vnitřní strukturou. Práce je rozdělena do 8 kapitol. První čtyři kapitoly stručně shrnují současný stav poznání v následujících oblastech: stavba kosti, požadavky kladené na syntetické kostní náhrady, vnitřní stavba kostních náhrad a způsoby jejich přípravy s důrazem na 3D tisk. Zbylé kapitoly tvoří experimentální část, kde byla nejdříve analyzovaná mikro/makro struktura myší kostry. Na základě naměřené velikosti pórů (50 – 200 μm) a dle literární rešerše bylo namodelováno 16 struktur majících rozdílný tvar, zakřivení a velikost pórů. Struktury byly vytištěny pomocí stereolitografie z disperze obsahující fosforečnan vápenatý. Slinuté keramické kostní náhrady měly z hlediska tkáňového inženýrství ideální strukturu, obsahovaly jak propojené makropóry (do 500 μm), tak i mikropóry (3 μm). Výsledky potvrzují, že stereolitografie je

vhodná, a oproti jiným technikám relativně přesná metoda, pro přípravu scaffoldů majících rozličnou vnitřní stavbu. Na strukturách vytištěných pomocí stereolitografu bude v budoucnu možné nezávisle studovat jednotlivé parametry ovlivňující chování náhrad v těle a posunout tak poznání v oblasti léčby rozsáhlých poškození kostry.

KEYWORDS

3D printing, ceramics, scaffold, bone structure, architecture, porosity

KLÍČOVÁ SLOVA

3D tisk, keramika, nosič, struktura kosti, architektura, porozita

NOVOTNÁ, L. *3D tisk keramických kostních náhrad s rozdílnou vnitřní stavbou.* Brno: Vysoké učení technické v Brně, Fakulta elektrotechniky a komunikačních technologií, 2017. 49 s. Vedoucí bakalářské práce prof. Ing. Ivo Provazník, Ph.D., Ing. Josef Jaroš, Ph.D., Doc. Jana Kolářová, Ph.D.

DECLARATION

I declare that I have written the bachelor thesis titled "3D printing of ceramic bone grafts with different internal architecture" independently, under the lead guidance of Josef Jaros and further cooperation with Ivo Provaznik and Jana Kolarova, and using the technical literature and other sources quoted within the thesis and detailed in the list of literature in the final section.

As the author of the thesis, I furthermore declare that, as regards the creation of the work, I have not infringed any copyright. In particular, I confirm that I have not violated anyone's personal and/or ownership rights and I am fully aware of the consequences of breaking Regulation § 11 of the Copyright Act No. 121/2000 Coll., as amended, and intellectual property rights or changes in related Acts (the Intellectual Property Act), as amended, inclusive of possible consequences resulting from the provisions of the Criminal Act No. 40/2009 Coll., Section 2, Head VI, Part 4.

Brno ....

Ing. Lenka Novotná, Ph.D

ACKNOWLEDGEMENT

First of all, I would like to thank my supervisor prof. Ing. Ivo Provazník, Ph.D and consultant doc. Ing. Jana Kolářová, Ph.D for their guidance, this thesis could not have become a reality without them. Also, I would like to express my great gratitude to my consultant Ing. Josef Jaroš, Ph.D. for planning the experiments and for helping me during the work. His advice has been always very useful. I am looking forward to the next cooperation.

Furthermore, many thanks go to prof. RNDr. Jaroslav Cihlář, CSc and the Central European Institute of Technology (Brno University of Technology) for the possibility of using their 3D printer and for providing the consumables necessary for the experiments.

CONTENT

LIST OF FIGURES

LIST OF TABLES

INTRODUCTION

Defects and functional disorder of bone is a long-time global health care problem. Healthy bone has the capacity for regenerative growth and remodelling, however repair and regeneration of large bone defects caused by disease, trauma or tumour resection remains a significant clinical challenge. Bone disorders are of significant concern due to increasingly active lifestyles, accidents, obesity and population ageing. Bone graft is the second most transplanted tissue, right after the blood. More than 2.2 million bone grafting procedures were performed in 2005 worldwide [1] in order to repair bone defects in orthopaedics, maxillofacial surgery and dentistry; and it can be assumed that ever since the demand have grown steadily.

Current medical treatments of bone defects have been largely focused on the replacing the lost bone with autogenous (gold standard) or allogeneic bone grafts. Using autografts (parts of bone harvested from the patient's own body, usually from an iliac crest) is limited by quantity and quality of available bone, in addition to that, there is a risk of donor side morbidity associated with the harvesting. Using of allografts (bone grafts taken from a donor, usually from a bone bank) often lead to postoperative infection and fracture and also there is the potential risk of disease transmission and immune rejection. Synthetic bone grafts are being viewed as a potential alternative to the conventional bone grafts, mainly due to their limitless supply and no disease transmission.

An interdisciplinary field dealing with the development of the biological substitutes that restore, maintain, or improve function or a whole organ is called tissue engineering (TE) [2]. It combines knowledges of materials science and engineering, cell biology, and regenerative medicine. Nowadays bone tissue engineering (BTE) focuses on the regeneration of damaged bone instead of replacing it. Essential for BTE is the scaffold, a three-dimensional porous and biodegradable structure guiding the new tissue formation by supplying a matrix with interconnected porosity and tailored surface chemistry for cell attachment, proliferation, differentiation and the transport of nutrients and metabolic waste. Among various kinds of biomaterials, bioactive ceramics are being considered as the most suitable material for BTE applications.

It is challenging to design the "ideal scaffold" because the requirements (e.g. large interconnected pores, controlled resorption rate, sufficient mechanical properties, etc.) are manifold and often contradictory. The production of geometrically controlled, reproducible structures and the independent variation of individual geometric parameters are crucial. Current progress in additive manufacturing technologies has brought new opportunities in scaffold formation especially lithography based ceramic manufacturing (LCM) technology is promising because it allows the production of high-performance ceramic parts and possibility of systematic studying of scaffold architecture parameters. In general, additive manufacturing has a great application potential due to possible customization of bone graft substitute. Not only outer shape, but also internal architecture can be personalized according to the individual patient needs.

This thesis aims to review current state of the art in the bone tissue engineering field, with emphasis to the internal scaffold architecture. Further, through the

possibility of using high resolution (~40 μm) ceramic stereolitograph, another objective was to design and print ceramic scaffolds having controlled internal structure which was so far unachievable by other methods. It would be great if this work contributed to improve scientific knowledge and helped with dealing with one of the current global health care problems – regenerating of large segmental bone defects.

1. BONE

Since the thesis deals with bone substitutes, bone composition, structure, and basic properties will be briefly describe for better understanding. The term bone may refer to both an organ and more specifically to bone tissue. While bones as organs consists of bone tissue, bone marrow, blood vessels, epithelium, and nerves, the description will be mainly focused on a concept of bone tissue consisting of bone mineral matrix and bone cells [3-5]. The bone performs a number of important functions in the organism which can be classified into three categories: (1) mechanical functions (structural support for the mechanical action of soft tissues, protection of soft organs and tissues, (2) synthetic functions (a source of cells that produce red and white blood cells), and (3) metabolic functions (mineral and fat reservoir, role in acid-base balance) [6].

1.1. Bone tissue composition

Bone is a mineralized connective tissue that exhibits four types of cells: osteoblasts, bone lining cells, osteocytes, and osteoclasts [7]. The basic building blocks are (1) macromolecules (~25 wt.%), of which type I collagen is the major constituent, (2) small plate-shaped crystals of apatite (~50 wt.%), and (3) water (~25 wt.%) [3, 8]. The hydroxyapatite crystals give bones their hardness and strength, while the collagen fibers give them flexibility. Combination of these components forms extremely tough, yet lightweight, adaptive and multi-functional material.

1.1.1. Mineral phase and collagen framework

The mineral phase forms about two thirds of the weight of a dry bone, or half of its volume [3]. Bone mineral, sometimes called "bioapatite", can be considered as an impure form of hydroxyapatite (HA, $Ca_{10}(PO_4)_6OH_2$) with a variable Ca/P molar ratio of 1.6–1.7 [9] and significant and varying amounts of carbonate and hydrogen phosphate ions [10, 11]. In addition to that, the apatite lattice is prone to substitutions (by F^-, Cl^-, Na^+, K^+, Fe^{2+}, Zn^{2+}, Sr^{2+}, Mg^{2+}), vacancies, and solid solutions [12]. A bone apatite contains about 7–7.5 wt% of carbonate which dominantly substitutes PO_4^{3-} ion [3, 12, 13]. The carbonate-containing apatite has higher solubility compared to the hydroxyapatite as the $Ca–CO_3^{2-}$ bond is weaker than the $Ca–PO_4^{3-}$ bond. Furthermore, the presence of substituting ions results in nanocrystalline platelets morphology of biologically produced apatite [12]. The documented dimensions of apatite crystals in bone are following: the length of 30–50 nm, width of 15–30 nm and thickness of 2–10 nm [14, 15].

About one third of weight of the dry bone is formed by the tough matrix, mainly composed of collagen fibers (~90%), non-collagenous proteins, glycosaminoglycans and lipids [16]. Detailed description of collagen structure can be found in chapter 1.2.

1.1.2. Bone cells

Bone cells are crucial for the function of bones. In particular, bone cells are responsible for a continuous remodelling process that responds to mechanical forces and that results in the coordinated resorption and formation of new bone tissue [8]. The scheme is shown in Fig. 1. Osteoclasts, cells which differentiate from hematopoietic progenitor cells of the monocyte and macrophage lineage [8], are found on bone surfaces and are responsible for bone resorption. Osteoblasts (comprising 4–6% of the total resident bone cells) cause the formation of new bone tissue [7]. Osteoblasts are cuboidal cells, derived from mesenchymal stem cells. They actively synthesize extracellular matrix on bone surfaces which is subsequently mineralized. Osteoblasts entrapped in matrix differentiate into osteocytes. They are the most abundant (comprise 90–95% of the total bone cells) and long-lived cells, with a lifespan up to 25 years [17]. Osteocytes are located in lacunas, surrounded by bone tissue. They can communicate with each other and receive nutrients via long cytoplasmic processes that extend through canaliculi, channels within the bone matrix. Osteocytes should be ideally distributed to sense external mechanical loads and to control the process of adaptive remodelling by regulating osteoblast and osteoclast function [18]. Other osteoblasts which remain inactive on the surface of the new bone and protect the underlying bone are known as lining cells.

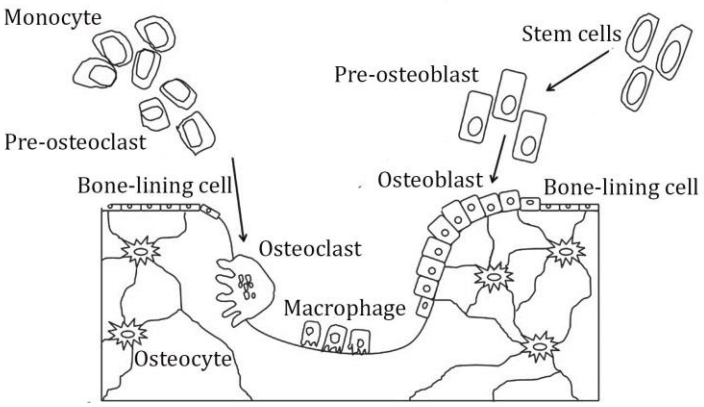

Fig. 1. A schematic illustration of different types of bone cells and their precursors during bone remodelling process. Figure adapted and modified from ref. [8].

1.2. Hierarchical structure of human bone

Bones exhibit a complex multi-scale hierarchical structure (see Fig. 2) which provides unique mechanical, chemical and biological functions. At least five levels of organization from the individual collagen molecules and mineral platelets to the whole bone can be distinguished [11, 15, 16, 19, 20].

At the sub-nanostructure level the bone is composed of organic (mainly type I collagen) and inorganic (hydroxyapatite) components [3]. Collagen consists of two α_1 and one α_2 polypeptide chains about 1050 amino acids long wound together in a triple helix, tropocollagen, with an average diameter of around 1.5 nm, and length of 300 nm. Tropocollagen molecules are self-assembled into microfibrils, exhibiting a periodicity of 67 nm and 35 nm cavities or orifices between

the edges of the molecules [15, 21-23]. The controlled nucleation and growth of apatite crystals take place at these voids. Further mineralization occurs on the surface of the fibril forming a mineralized collagen fibril. These fibrils associate with each other to form arrays of aligned fibrils that make up a larger structure called the fibre. Fibres then assemble into different patterns, in mature bone most often into lamellae [15] (~5 μm-thick sheets) which at microstructure scale further form osteons and trabeculae [16]. In humans, osteons are several millimetres long with a diameter from 150 to 350 μm [24]. Inside of osteon, there is a central vascular channel, the Haversian canal (~90 μm in diameter). At the outer limits of the osteon there is a 5-μm thick cement line, which separates individual osteons. The spaces remaining between adjacent osteons are filled with interstitial lamellae, fragments of previous Haversian systems. [3, 11, 15, 23]. Analogous to an osteon in the cortical bone, the basic structure component of cancellous bone is the trabecula, which consists of lamellae sheets with osteocytes between them [25]. Trabeculas are arranged along stress lines. The macroscale level represents the overall shape of the bone. Bone can be compact (cortical, dense) or cancellous (trabecular, spongy). Compact bone is almost solid, with 5–30 % (typically 10%) porosity, whereas porosity of cancellous bone varies between 30–90 % (typically 50-90%) [26, 27].

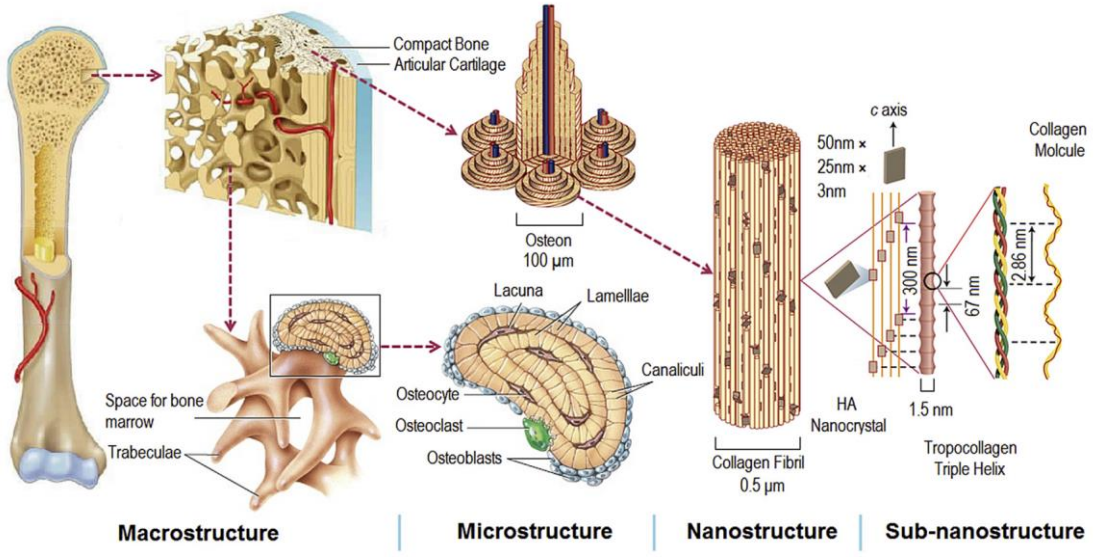

Fig. 2. Hierarchical structure of bone. Image adapted from ref. [28].

1.3. Mechanical properties of bone

The most important mechanical parameters of bone are Young's modulus (measure of a stiffness), strength, and fracture toughness; however, their determination is quite challenging. Bone properties vary with skeletal site, age, gender, mechanical loading, preservation of samples, mineral and water content, and so on [29]. The properties are moreover anisotropic, cortical bone is stronger and stiffer if loaded longitudinally along the diaphyseal axis, whereas fracture toughness is higher in the transverse direction. Mechanical properties depend especially on the bone matrix porosity and degree of mineralization [29], in case of cancellous bone they depend also on the architectural arrangement of the

individual trabeculae. The fracture toughness of living bone (cortical 2-12 MPa·$m^{1/2}$ [30], cancellous 0.1–0.8 MPa $m^{1/2}$ [31]) is excellent, the fracture energy is almost comparable to steel [32]. Explanation of toughening mechanisms in bone is beyond the scope of this thesis and can be found elsewhere [33]. The values of Young's modulus and compressive strength of human bone are summarized in Table 1. Other mechanical properties of bone and description of testing procedures can be found in one of Keaveny's interesting publications [27, 34].

Table 1. Young's modulus and compressive strength of bone (average values from [27, 30, 32, 35, 36]).

Bone	Density ($g \cdot cm^{-3}$)	Young's modulus (GPa)	Compressive strength (MPa)
Cortical bone, longitudinally	2.5	11–21 (up to 55)	70-280
Cortical bone, transversely	2.5	5–13	~ 50 (up to 150)
Cancellous bone	0.2-2	0.01–0.5	0.2-20

2. SYNTHETIC BONE GRAFT

Replacement of damaged bone has been an important clinical challenge. Concerns related to the use of autografts and allografts has led to the search for alternatives, so during the past 50 years a variety of synthetic bone graft has been developed. The first generation of biomaterials included bioinert materials whereas biomaterials of the second generation were either bioactive (able to interact with the biological environment to enhance the biological response and the tissue/surface bonding) or resorbable (able to degrade while new tissue regenerates and heals). The third generation (since 2000s) of biomaterials has been designed to stimulate specific cellular responses at the molecular level [37]. That generation is characterised by having used bioactive and resorbable materials as temporary three-dimensional porous structures which have been able to activate genes of cells that stimulate regeneration of living tissue. For these biomaterials, the bioactivity and biodegradability concepts are combined with the aim to develop such materials that will help the body heal itself.

An ideal bone graft material should exhibit the following four characteristics: (1) osteointegration (the ability to chemically bond to the surface of bone without an intervening layer of fibrous tissue); (2) osteoconduction (the ability to support the growth of bone over its surface); (3) osteoinduction (the ability to induce differentiation of stem cells from surrounding tissue to an osteoblastic phenotype); and (4) osteogenesis (the formation of new bone by osteoblastic cells present within the graft material). Only autogenous bone graft satisfies all of these requirements [38].

2.1. Bone scaffold requirements

An ideal bone scaffold should possess multiple characteristics [38]. It must be biocompatible (e.g. must not elicit an inflammatory response nor induce immunogenicity or cytotoxicity). Usually three dimensional porous structures are produced with regard to support tissue formation, adhesion and migration of cells throughout the material and to allow vascularization of the ingrown tissue. Pores should be interconnected with pore size at least 100 μm in diameter [39, 40]. How pore size and shape affect the rate of bone apposition is discussed in detail in chapter 3. Besides macropores, microporosity of the walls is desired since it provides larger surface area for protein adsorption, cellular adhesion and proliferation [40, 41]. Scaffolds should be able to form a stable interface with the host bone without fibrous connective tissue. In addition, material should be degradable with resorption kinetics equal to the bone repair rate in order to facilitate load transfer to newly developing bone. The by-products must not be toxic and must be easily metabolised or eliminated by excretory organs [42]. From a mechanical point of view, synthetic scaffold should have a similar mechanical properties to those of the bone being replaced. The optimal Young's modulus of scaffold replacing cancellous bone should be in range 0.1–2 GPa [43] to avoid undesirable stress shielding effect. Initial strength must be sufficient for safe

handling during sterilization and surgery procedure, as well as scaffold must withstand physical forces *in vivo*. Finally, scaffolds should be easily manufactured in complex shapes which match the bone defect. To sum up, synthetic bone grafts should ideally mimic the native bone in both mechanical and osteogenic properties.

2.2. Scaffold composition

A variety of artificial materials have been used over the centuries to fill bone defects. Metals has superior mechanical properties and therefore are suitable for load bearing applications, however, their biocompatibility is not satisfactory, tissue adherence is poor and risk of toxicity is high due to accumulation of released metal ions in the body [28, 40, 43]. On the contrary, polymeric materials can behave both bioactive and resorbable *in vivo*, but for using as a bone scaffold they have insufficient stiffness and compressive strength [40, 44, 45]. As was mentioned in chapter 1.1, bone is two-thirds composed of ceramics, therefore ceramics seems to be the optimal choice. Calcium phosphate based ceramics and bioglass exhibit excellent biocompatibility, and high osteointegrative and osteoconductive properties. Bioglass is composed of various proportions of SiO_2, Na_2O, CaO and P_2O_5. It has the ability to degrade at a controllable rate and convert to an HA-like material, to bond firmly to hard and soft tissues, and during the degradation process to release ions which have a positive effect on osteogenesis and angiogenesis [46]. Compared to calcium phosphates, bioglass has worse mechanical properties and it is more complicated to fabricate porous 3D scaffolds. Further information can be found in the literature written by the bioglass inventor prof. Hench [37, 41, 47].

2.3. Calcium phosphates

Calcium phosphates (CaP) form a wide class of tuneable bioactive ceramics used for bone tissue regeneration. Most of them are osteoconductive and some of them also osteoinductive. They can promote bone growth *in vivo* [48], and recruit bone marrow stromal cells (BMSCs) to ectopic sites to induce bone formation [49]. The biological effect of individual CaP are related to subtle differences in their physical and chemical properties, such as solubility, crystallinity and stoichiometry (e.g. Ca/P ratio) [50]. Diverse combinations of CaO, P_2O_5 and water provide a large variety of calcium phosphates with Ca/P ratio ranging between 0.5 and 2. The most known and used are hydroxyapatite (HA), β- and α -tricalcium phosphates (β-TCP, α-TCP), amorphous calcium phosphates (ACP), calcium-deficient hydroxyapatite (CDHA) and their combination (BCP) [51, 52]. The lower the Ca/P molar ratio is, the more acidic and water-soluble the calcium orthophosphates are [52]. The dissolution rate of calcium phosphates decreases in the following order: ACP > α -TCP > β -TCP > crystalline HA [30, 53]. The degradation products of CaP can be used for new bone formation [51]. The solubility and osteoinductive potential of selected CaP are summarized in the Table 2.

Table 2. Properties of CaP that influence osteoblastic differentiation.

Name	Ca/P ratio	Solubility (K_{sp})	Osteoinductivity
Hydroxyapatite	1.67	Poor (10^{-58})	+
Tricalcium phosphate	1.5	Fair (10^{-25}–10^{-29})	++
Amorphous CaP	1.15–1.67	High (10^{-23}–10^{-25})	+++
Biphasic CaP	1.5–1.67	Depends on TCP/HAP ratio	++++

2.3.1. Hydroxyapatite

The composition of HA is the closest to that of bone mineral. Crystalline HA is considered to be osteoconductive but not osteoinductive. It is the least soluble phase among CaPs [54]. Its dissolution rate is depended on the crystallinity, porosity and composition (impurities) of the HA phase; type, concentration and pH of the solution, degree of the solution saturation and solid/solution ratio. Despite low solubility HA surfaces can provide nucleating sites for the precipitation of apatite crystals in culture medium [55]. Compared to a cortical bone, compressive strength of synthetic HA is higher, however, fracture toughness is significantly lower due to missing collagen fibres [30].

2.3.2. Tricalcium phosphates

Tricalcium phosphates (TCP, $Ca_3(PO_4)_2$) occur in two crystallographic phases: α and β. β–TCP is stable at room temperature and transforms into α–TCP phase at 1125 °C [56]. α–TCP is thermodynamically metastable, but it can be retained during cooling to room temperature. Both phases have different structure, density and solubility (K_{sp} values of $10^{-25.5}$ for α–TCP and $10^{-28.9}$ for β–TCP [50]. They are used in several clinical applications: β–TCP as the component of commercial bioceramics, whereas α–TCP as the major constituent of bone cement [53]. More extensively used β–TCP is considered to be both osteoconductive and osteoinductive. Due to the low interfacial energy with respect to apatite, it can provoke the precipitation of the apatite layer upon incubation in aqueous ionic solutions [55]. The compressive and tensile strength of porous β–TCP is similar to that of cancellous bone [57]. α–TCP is also osteoconductive and osteoinductive. It is more soluble than β–TCP; due to a higher specific energy it can be hydrolysed to CDHA in aqueous solutions [58]. However its quick resorption rate (faster than formation of a new bone) limits its application as single phase ceramics.

2.3.3. Biphasic (multiphasic) calcium phosphates

Calcium phosphates might form biphasic, triphasic and multiphasic compositions. The main idea of this concept is to combine more stable calcium phosphate phases (e.g., HA) with the more soluble and osteoinductive phases such as TCP. Among all known BCP formulations, BCP consisting of HA and β-TCP is the best investigated. It is soluble and gradually dissolves in the body, seeding new bone formation as it releases calcium and phosphate ions. Nevertheless, BCPs can be composed of α-TCP and β-TCP or can be triphasic consisting of HA, α-TCP and β-TCP [59]. BCPs can be produced physically by mixing HA and TCP or by sintering non-

stoichiometric or stoichiometric calcium phosphates at temperatures above ~700°C (~1300°C, respectively) [52]. The major properties (such as bioactivity, resorbability, osteoconductivity and osteoinductivity) of the bi(multi)phasic compositions depend greatly upon the characteristics of the individual phases and can be tuned by changing their relative amounts.

3. ARCHITECTURAL PARAMETERS OF SCAFFOLDS

Recent advances in bone tissue engineering have emphasized the need for properly design of scaffolds to allow cells to attach, migrate, proliferate and differentiate. At the first stage after the implantation, the composition and surface chemistry play the pivotal role, as they influence the ability of cells to initially attach. In the second step, a proper architecture of the scaffold become more important, because it controls the cell ability to migrate, allows nutrients and oxygen to flow into the scaffold and hence to help regenerate the tissue.

The most important structural parameters are pore size, pore size distribution, interconnectivity and pore morphology (shape and curvature). Fig. 3 correlates the structural parameters with their effect on the mechanical and biological properties of the scaffold.

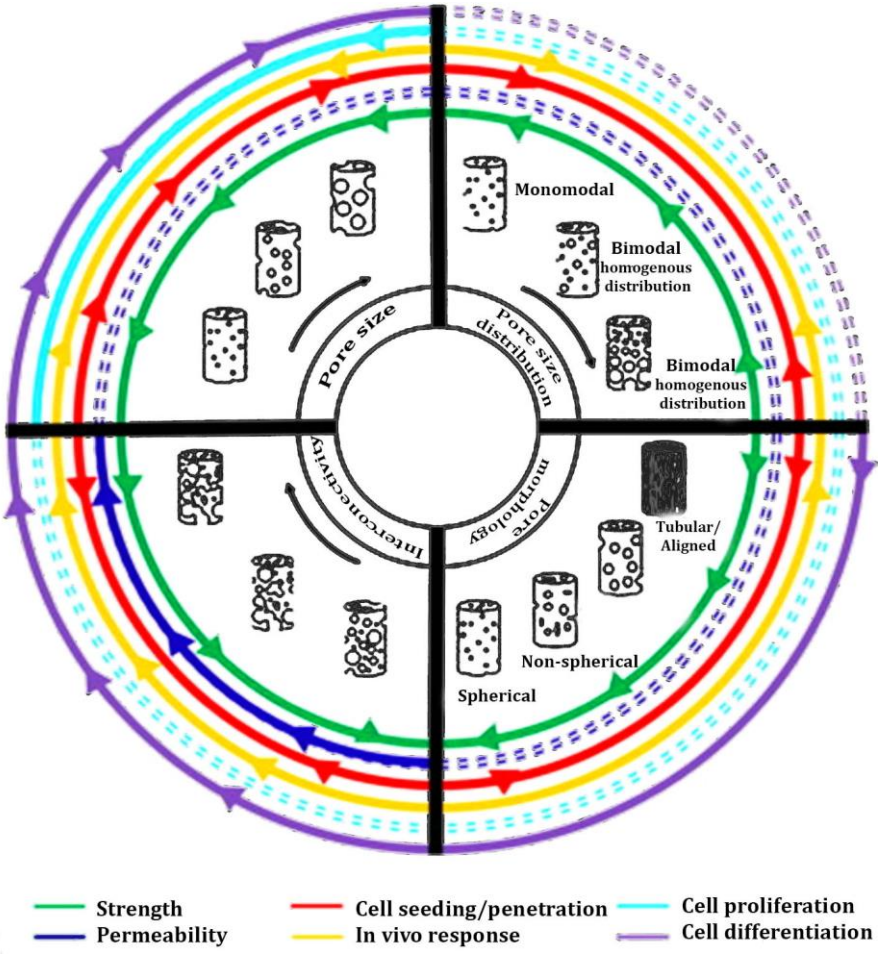

Fig. 3. A scheme summarizing the influence of structural properties on the physico-chemical and biological performance of the scaffold. Image adapted and modified from ref. [60].

The black internal arrows indicate the increase of the structural property whereas the coloured lines represent the physico-chemical (mechanical properties, permeability) and biological (cell seeding/penetration, *in vivo* response, cell proliferation and cell differentiation) properties. The coloured arrows indicate a trend, whereas the dashed lines controversy or a not determined

trend. As the scheme suggests, the individual characteristics are often contradictory depending on the structural parameters. [60]. For example, the higher the pore size, the better cell seeding and differentiation, and the worse the mechanical strength. Basically, the higher the strength, the worse is the biological response of the scaffold. It suggests that it is impossible to define single architecture that would be optimal and meet all scaffold requirements. The individual structural parameters are discussed in the following subchapters.

3.1. Pore size

Porosity is defined as a volume of void spaces within a material. According to the International Union of Pure and Applied Chemistry (IUPAC) the porosities of dense materials are classified in three different types: micropores (< 2 nm), mesopores (2–50 nm) and macropores (> 50 nm). Nevertheless, the classification for tissue engineering is different, the biomaterial scientists usually classify pore sizes as macropores (> 50 μm) and micropores (< 10 μm) [60]. Pore sizes can be determined by several techniques, such as mercury porosimetry, nitrogen adsorption, eventually by many image methods based on data taken from: μCT (micro-computed tomography, SEM (scanning electron microscope), or AFM (Atomic Force Microscopy). Due to the different physical nature of each method, it should be borne in mind that the measured values tend to slightly differ and cannot be directly compared.

3.1.1. Microporosity

Micropores are in tissue engineering usually defined as small pores with a diameter below 10 μm [60, 61]. The microtopography, encompassing both surface roughness and microporosity, can be influenced by the processing technique, by sintering conditions and by polishing. Micropores are divided into open and closed. If they are closed, i.e. isolated within a solid, they influences overall mechanical properties like strength and modulus of elasticity with implications for cell mechano-transduction [62]. However, they have only negligible effect on biological performance of the scaffold. With respect to the effect of open microporosity on bone formation and cell behaviour, the results vary depending on whether they were obtained *in vivo* or *in vitro* [63]. Many of *in vivo* studies [62, 64-66] have shown positive effect of the open microporosity on the scaffold biological performance after the implantation. For instance, the increased levels of microporosity led to formation of higher volumes of denser bone early after the implantation compared to non-porous implants [62]. Another study [64] confirmed that microporosity was absolutely necessary for osteoinduction.

Several mechanisms how microporosity affects the cell and tissue behaviour have been reported: (1) Microporosity allows cells to spread and invade the material by providing anchoring sites for cell extensions (filopodia) [67]. (2) Microporosity enhances selective adsorption of serum proteins which subsequently positively influences cell adhesion and proliferation and thus improves general cell behaviour [68, 69]. E.g. comparing dense and microporous HA revealed a 10-fold increase in protein adsorption on the surface of microporous HA after 30 min of immersion in a complete culture medium [70]. (3) Positive

effects of open interconnected microporosity in early stages post implantation are connected to higher vascularization of the scaffold due to the higher nutrition permeability [62]. (4) The highly microporous scaffolds exhibit large specific surface area resulting in faster dissolution and reprecipitation of calcium and phosphate ions leading to the formation of biological apatite. Proteins that are co-precipitated in that process induce the differentiation of cells into the osteogenic lineage [64].

The ability effect of surface microtopography to bind various amount of serum proteins (bone morphogenic proteins – BMPs; laminin, fibrin, fibronectin) is illustrated in Fig. 4. Cells interact with biomaterials directly through the transmembrane proteins – receptors, or via proteins adsorbed on surface of materials [71]. The higher surface microporosity / roughness is related with the larger focal adhesion sites of cells, alternatively higher cellular attachment, spreading and interaction with the biomaterial. Additionally, the orientation and conformation of protein molecules adsorbed on the surface are critical for cells to recognize specific bioactive domains of adsorbed proteins which initiate signalling events. Subsequently, these biomolecular signals strongly influence cellular behaviour such as adhesion, morphology, migration, proliferation and differentiation [60].

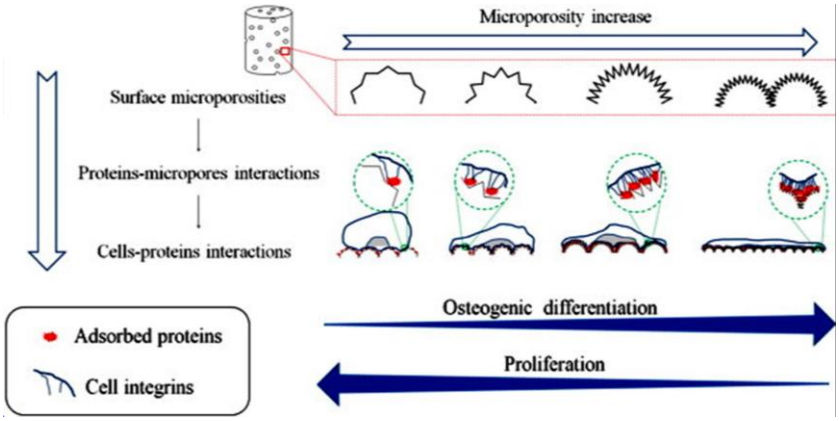

Fig. 4. Scheme correlating microporosity of biomaterials with the cell behaviour [60].

3.1.2. Macroporosity

Bone tissue regeneration is believed to be mostly affected by macroporosity. The influence of scaffold pore size on bone tissue regeneration have been studied for a long time, however, no uniform conclusion about an optimum pore size has been reached yet. Almost fifty years ago, Klawitter and Hulbert [72, 73] advised that scaffolds should be porous with a minimum pore interconnection size of 100 μm, since then no great progress has been made. In the highly cited review on this topic, released in 2005, Karageorgiou and Kaplan [61] recommended pore size above 300 μm for cell migration and proliferation. They also reported that the optimal porosity was different when comparing *in vitro* studies with *in vivo* studies. The lower macroporosity may be beneficial *in vitro*, because cell proliferation is controlled and cell aggregation could be forced when the porosity is lower. Joly [74] studied the pore filling process by human fibroblasts depending on incubation time and the scaffold pore size (60-120, 120-180, >180 μm). Fig. 6

shows that after one day, human fibroblasts were fully spread on the scaffold walls and after 7 days, full pore filling was observed on all samples, however, it seems that the pore filling was more complete for smaller pore sizes.

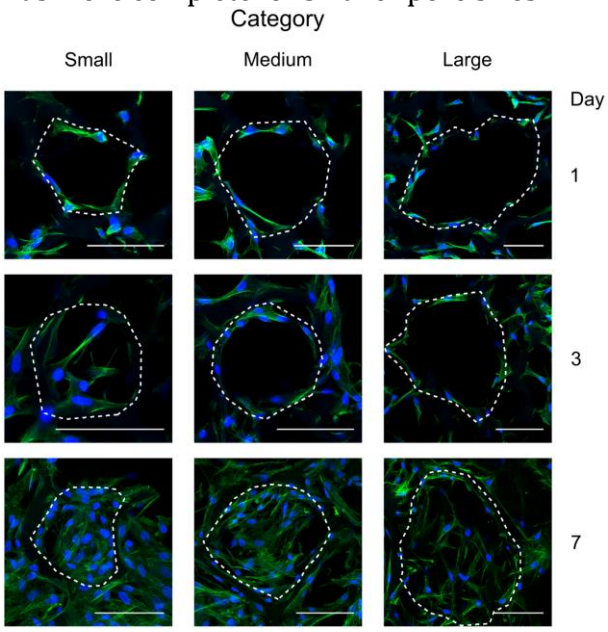

Fig. 5. The pore filling behaviour of fibroblasts for three pore size categories for 7 days. Actin cytoskeleton – green; cell nuclei – blue. Scale bar equals 100 mm. Adapted from [74].

Contrary, larger pores may be advantageous *in vivo*, because they could stimulate bone regeneration [61]. Feng studied the effect of macropores with a constant interconnection size of 120 μm on fibrous tissue invasion and the formation of blood vessels after 4 weeks *in vivo* after implantation. He reported that the amount of formed fibrous tissue decreased with the increasing pore size (Fig. 6a). A comparison of the blood vessels area (Fig. 6a) shows that the pores smaller than 400 μm (Fig. 6a) could considerably limit blood vessel formation, allowing formation of only smaller vessels, whereas bigger pore sizes, i.e. 400–700 μm (Fig. 6b) allowed proper new blood vessel formation [75].

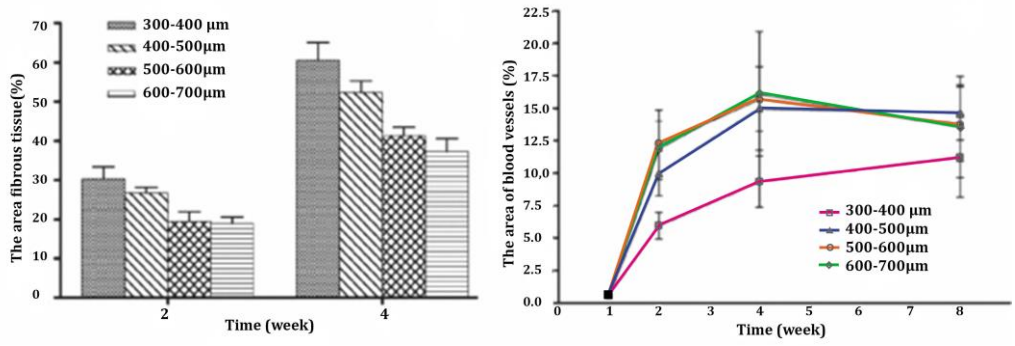

Fig. 6. Effect of macropores (300–700 μm) in β-TCP on fibrous tissue invasion and the formed blood vessels post implantation. (a) The area of fibrous tissue (%) in macroporous scaffolds with constant interconnection (120 μm) and different pore sizes at 2 and 4 weeks. (*b*) The area of blood vessels (%) in macroporous scaffolds with constant interconnection (120 μm) and different pore sizes at 1, 2, 4 and 8 weeks. Figure adapted and slightly modified from ref. [75].

3.2. Pore morphology – curvature and geometry

Regardless of the total pore size, pore shape strongly influences the biological response. The effect of curvature is evident both in the nanometer range and at the single cell level. At the nanometer range, it is related with surface topography [76] and it is discussed in chapter 3.1.1. At the macropore scale, the type of curvature, is important, however, there is still missing a consensus about what kind of curvature is the best for tissue regeneration.

Many studies agreed that the tissue growth process prefers concave surfaces to convex and flat ones [76-79]. Rumpler [80] showed that curvatures with radii much larger than the cells could interact with the cells and influence their behaviour. Murine osteoblast-like cells were cultured on hydroxyapatite channels with triangular, square, hexagonal, and circular cross sections (see Fig. 7). Results showed that the initial tissue formation occurred at corners; cells on edges were not growing until a growth of adjacent tissue resulted in a curved environment [80]. Tissue growth was thus curvature-driven; the growth increased with local curvature which led to a round opening regardless of the initial substrate shape as is evident in Fig. 7a. Also the numerical model which simulates development of tissue formation due to ongoing culture time was proposed (see Fig. 7b).

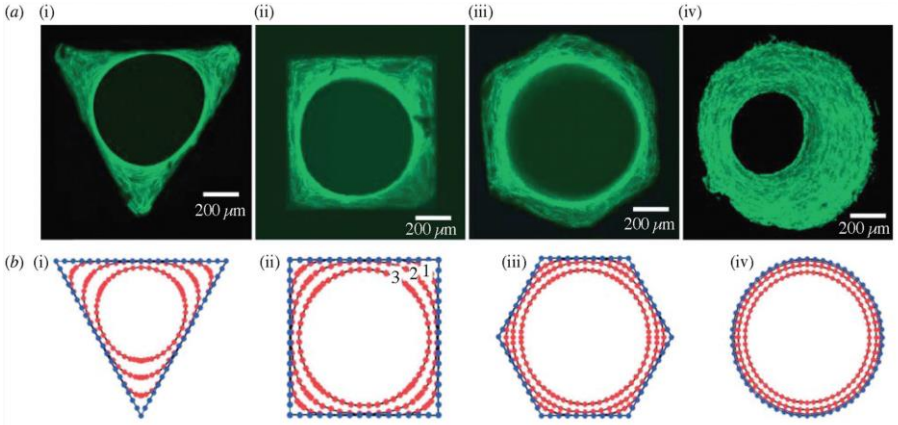

Fig. 7. (a) New tissue formation in three-dimensional matrix (Actin stress fibres stained green); (b) Numerical simulation of tissue formation within channels of various shapes. Adapted from ref. [80].

Although majority of the studies were performed *in vitro*, some *in vivo* experiments confirmed the role of curvature in the bone-tissue-regeneration process. A histological study that compared the amount of blood vessels inside concavities and around convexities (see Fig. 8a,b) of an implant in a rabbit model shown that blood vessels were concentrated in the first weeks after implantation in concavities [81].

Fig. 8d shows the distribution of actin fibres and myosin IIb in cells adhered on the local curvature. The density of the actin fibre and myosin IIb was found to be higher on concave surfaces, which indicates a locally higher state of cell adhesion and thicker cytoskeletal formation in the concave surfaces surroundings. Furthermore, it has been reported that variation in the surface curvature could significantly affect the cell attachment rate, cell migration speed, and cell morphology including the cell spread area [76, 78].

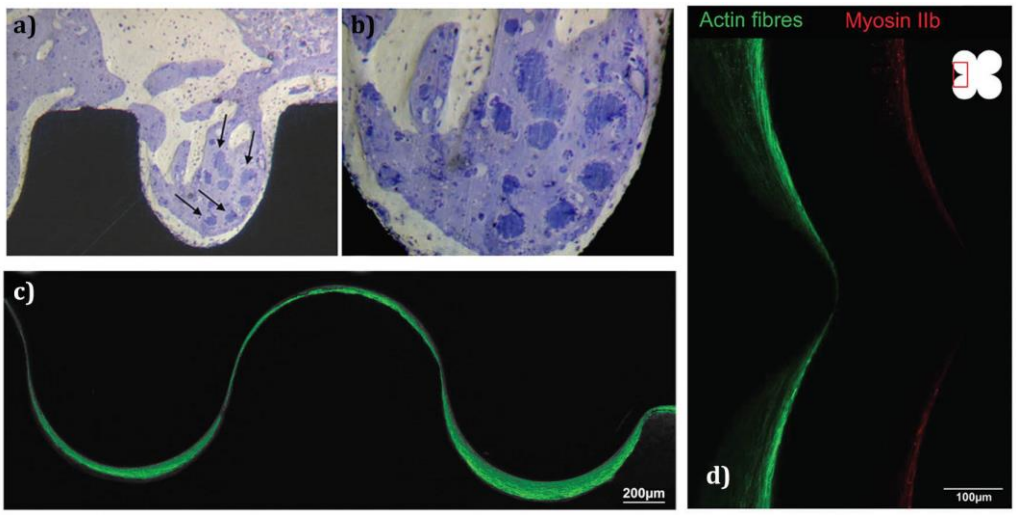

Fig. 8. Comparison of convex and concave curvature and their influence on tissue formation *in vivo* and *in vitro*. Blood vessels (indicated by arrows) are generated in the concavities on the surface of an implant (a and b). *In vitro* results show much larger volumes of generated tissue on concave surface compared to convex ones (c). The density of both actin fibres and myosin IIb is dependent on the local curvature, it increases on the concave surface, suggesting locally higher states of cell stress (d). Adapted from ref. [76].

3.3. Interconnectivity and permeability

The permeability is closely related to the pore interconnectivity (defined by the size of connection between two different pores). Generally, a better bone penetration and higher vessel infiltration is observed if the scaffolds are more permeable, i.e. able to allow the circulation of a fluid (e.g. nutrients). The level of pore interconnectivity also significantly influences the resorption rate of scaffold as the presence of sufficiently large interconnected pores enable the invasion of blood vessels and cells, and thus biodegradation of material and bone ingrowth [51].

When using additive manufacturing techniques the pore morphology and interconnectivity of the porous structure can be precisely controlled. For example, a 3D-printed gyroid pore structure exhibited a 10-fold higher permeability compared to the pore architecture resulted from salt leaching [82].

Lu [83] studied *in vitro* and *in vivo* osteoblast colonization of CaP scaffolds with interconnections ranging from 30 to 100 µm, concluding that 40 µm large interconnections were being the most favourable interconnection size during *in vitro* tests. *In vivo* experiments revealed that pore interconnection of 20 µm were large enough for cell penetration, however, the size had to be over 50 µm to allow new bone ingrowth [83]. And even though, it is difficult to define the exact porosity characteristics for an ideal scaffold, Hing [65] assumed that a total porosity should be higher than 50–60 vol.%, an interconnection size should be higher than 50–100 µm and strut porosity should be higher than 20 vol.%.

3.4. Pore size distribution

The pore-size distribution is the relative abundance of each pore size in a representative volume of the material. Pore size distribution can be monomodal (pores of one size)/ bimodal/ polymodal and also homogenous/ heterogeneous/ gradient or random/organized. In general, scaffold pore size distribution should be at least bimodal containing both macropores for cells penetration and micropores for protein adsorption [60]. However, the optimal pore size distribution is still unclear. Some studies revealed [84] that scaffolds with a gradient porosity perform more efficiently than scaffolds with homogeneous pores.

3.5. Macroscopic pore arrangement – geometrical design of scaffolds

As well as the composition, the intrinsic structure plays critical roles in the success of a scaffold. Scaffold architecture design can significantly influence both cell behaviours and mechanical property (scaffolds of the same density but different design exhibit different strength). However, a general rule of unit cell selection and scaffold design is still missing.

Additive manufacturing has allowed an extensive control over the scaffold architecture (total porosity, the pore size and morphology, and pore size distribution). Nowadays the porous architecture is usually composed of periodically arranged structural units such as polyhedral units or point lattice designed through CAD. The geometrical shape of structural units can be simplify classified as truss, polyhedron and triply periodic minimal surface [85]. Cheah [86] proposed a library containing eleven types of unit cells (diamond lattice, cubic lattice, truncated octahedron, rhombic dodecahedron and rhombicuboctahedron) repeated regularly in 3D space only by joining vertices or edges and connected at faces.

Examples of frequently used scaffold architecture are shown in Fig. 9. The first unit cube is modelled by the solid tubular structures, perpendicular to each other and running in x, y, and z directions. The second “spherical” unit cube is formed by subtracting a sphere from a solid cube. The third “X” unit cube is formed by diagonally joining the corners of a unit cube with tubular. The less often used architectures trying to mimic the structure of trabecular bone, based on the freeform surface, are “diamond” and “gyroid” [87].

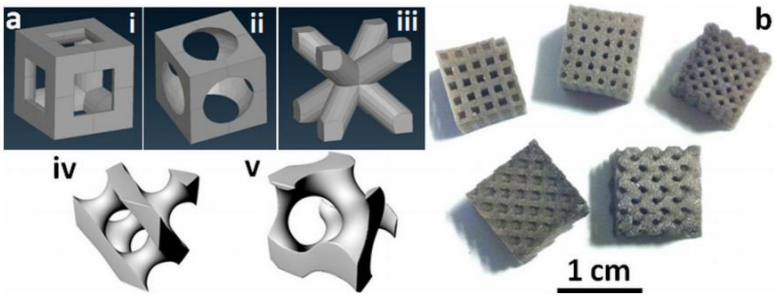

Fig. 9. CAD models and realization of the elementar units of five architectures: (a) Models of structures (i) cubic, (ii) spherical, (iii) „X“, (iv) diamond, and (v) gyroid; (b) printed bioglass scaffolds after sintering. Adapted from [87].

4. PROCESSING TECHNIQUES OF CERAMIC SCAFFOLDS

Traditionally, the goal of the processing of advanced ceramics has been to eliminate pores from the structure and thus improve the mechanical properties and overcome the inherent brittleness of ceramics. However, this concept is not valid in the case of ceramics intended for biomedical applications, because as mentioned earlier, multi-scale porosity is an essential parameter regardless of the worse mechanical properties. Porous ceramic bodies can be made by several traditional and newly developed techniques.

4.1. Partial sintering

Partial sintering is the simplest method suitable for processing of structures with randomly arranged irregular micropores. All ceramic materials are fabricated by thermal heating, at which the atoms diffuse across the boundaries of the particles, causing the particles fuse together. If the sintering temperature is too low or the dwell too short, the sintering is incomplete resulting in the residual porosity as shown in Fig. 10

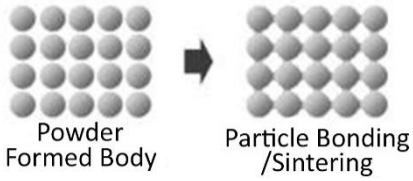

Fig. 10. Scheme of fabrication process by partial sintering. Adapted from [88].

The final pore size and porosity can be controlled by the particle size of the raw powder, by volume of the binder, by processing parameters, and, in particular, by the sintering conditions. The particle size of the starting powder should be two to five times larger than the desired pore size. The resulting porosity is usually lower than 50 % [88-90].

4.2. Traditional processing techniques

Macroporous ceramics have been fabricated by several traditional processing methods, the most commonly by the polymer replica, sacrificial fugitives, and direct foaming. The main principles of selected techniques are summarized in Fig. 11. The oldest one is the replica technique [91], which is based on the impregnation of the polymer foam with a ceramic slurry in order to obtain the ceramic structure exhibiting the same morphology as the original template (see Fig. 11a). Macropores prepared by this methods are highly interconnected with sizes between 150 μm and 3 mm, the overall porosity is high, varying between 40 % and 98 % [88, 90, 92]. Another traditional method is based on sacrificial template (see Fig. 11b) consisting of the preparation of a biphasic composite comprising a continuous matrix of ceramic particles and a dispersed sacrificial phase, which is subsequently extracted in order to generate pores within the sintered structure. The resulting ceramic structure is a negative replica of the original sacrificial template [90]. A freeze casting, where the liquid is the sacrificial phase, has also been extensively studied for application in bone tissue engineering

[93-98], mainly because of the ability to form porous lamellar structure with the incredible strength. The last traditional processing method is a direct foaming [99]. This technique is based on incorporation of a gaseous phase into a ceramic suspension through mechanical frothing or gas released by chemical reaction. The procedure, illustrated in Fig. 11c, allows a low-cost production of ceramic foams with the wide pore size distribution (10 – 300 μm) [90] and porosity (45 – 95 %), proportional to the amount of gas incorporated into the suspension.

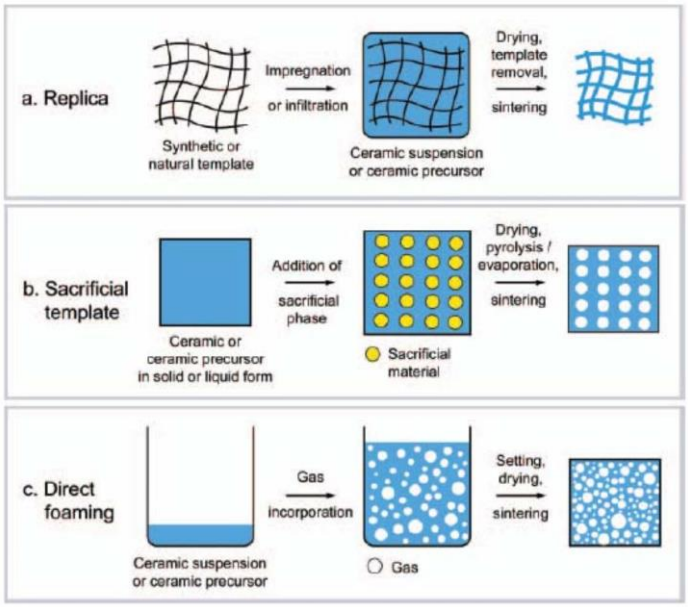

Fig. 11. A scheme of traditional processing routes used for the production of macroporous ceramics. Image adapted from ref. [90].

All these traditional processing techniques have in common that they are incapable to control the individual geometrical features separately. The size and shape of the pores and their interconnectivity are dependent on each other. For example, an effort to improve the mechanical properties of the scaffolds by reducing the total porosity usually cause the problems such a lack of interconnected pores or even lead to undesirable closed porosity. Moreover, the potential pore geometry is very limited and it is strongly dependent on the chosen processing techniques. Hence there has been a high demand for the development of new techniques which could have built various interior geometries required for tissue growth, so far difficult or even impossible to achieve through traditional processing techniques. Solid freeform fabrication can overcome the above mentioned weaknesses and thus it becomes a promising technique not only for application in bone tissue engineering.

4.3. Solid freeform fabrication

Solid freeform fabrication (SFF) (often referred as additive manufacturing - AM or rapid prototyping - RP) is a relatively new technique developed in 80's in the MIT. This method can quickly produce complex 3D objects without the need of using moulds or other forming or machining tools. Ceramic bodies are built directly based on the data generated by CAD systems.

The benefits of using solid freeform fabrication are numerous. First of all, it is possible to customize parts to be fabricated in order to fit the needs of individual patients. More specifically, an image of a bone defect can be acquired by e.g. computer tomography. A 3D CAD computer model is than developed from this scan. A common feature is that CAD model is sliced and ceramic body is build layer by layer [100, 101]. The control over the microstructure is better compared to traditional techniques. The size, shape, and location of internal features can be designed and fabricated according to the scaffold requirements. Besides that, additive manufacturing techniques are also very helpful in research, because they are capable to separate different geometrical parameters from each other and study them independently.

The most frequently used additive manufacturing techniques include: (1) 3D printing (3DP) or direct ink-jet writing, (2) selective laser sintering / melting (SLS / SLM), (3) stereolitography (SLA), (4) fused deposition modelling (FDM), (5) Robotic assisted deposition/robocasting, (6) Power-based 3D printing, (7) Laser assisted bioprinting (LAB), and (8) indirect techniques.

4.3.1. Three-Dimensional Printing

3D Printing (3DP) was developed in 1995 at the MIT [102]. The principle lies in printing of droplets of a binder fluid on a powder bed as is depicted in Fig. 12. The first thin layer of powder, such as calcium phosphate is smoothly dispersed on a building platform. A suitable binder is subsequently inprinted into the powderbed to bind the desired particles of the solid's cross section within the layer. Next layer is dispersed on top of the first layer. The printed binder binds the particles of the second layer together and to the previous bound layer. This process is repeated for every layer until the 3D structure is printed and the remaining powder is removed. Binder is finally extracted at high temperature during the consolidation [44].

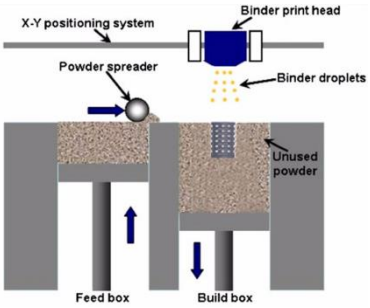

Fig. 12. Schematic drawing representing the 3D printing process. Adapted from [103].

The greatest benefits of the 3DP includes: broad material range, cost efficiency, no need of extra support structure. The main drawbacks are small green strength and problems connected with the depowdering due to the weak bonding between particles [104].

4.3.2. Selective laser sintering

Selective laser sintering (SLS), developed in 80's, works on a similar principle as 3D printing with the difference that the particles are not bonded by printed ink but

they are directly sintered using a high-power CO_2 laser beam which fuses the powder according to CAD data [44]. The main advantages are that no post processing and support material are needed. High processing temperature and possibility that powder could be trapped inside the printed body are the main disadvantages [104].

4.3.3. Stereolithography

The stereolithography process (SLA) is based on exposing a liquid photohardening polymer to ultraviolet rays as illustrates Fig. 13. An UV laser beam selectively initiates solidification in a thin layer of liquid photopolymer. The solidified layers are overlapped and cross-sectional structure is thus generated. It is the most accurate solid freeform fabrication method developed so far. Drawbacks are limited amount of material compositions. Support structure is needed if the structural components are not connected during the building [102].

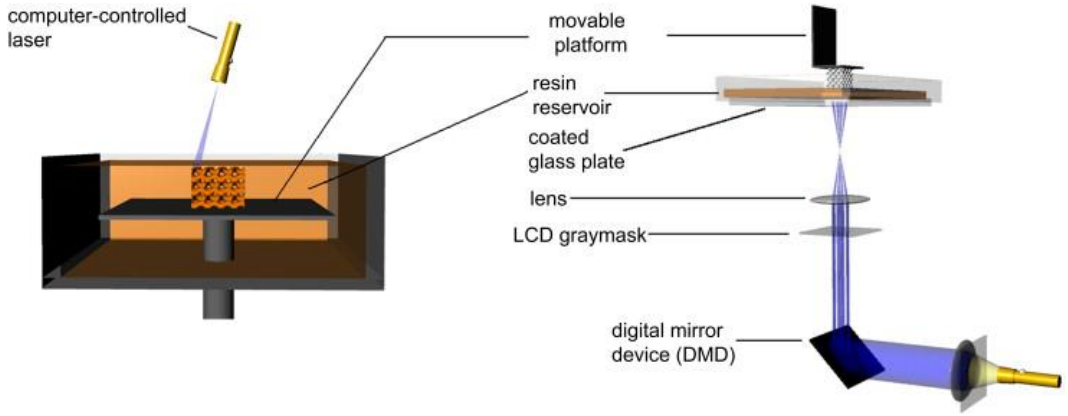

Fig. 13. Schemes of two types of stereolithography setups. Left: a bottom-up system with scanning laser. Right: a top-down setup with digital light projection [105].

4.3.4. Robocasting (RC)

Principle of the robocasting (RC) consists in the extrusion of an "ink" (here ceramic paste) through a nozzle. Robot controlled nozzle writes a paste directly layer by layer according to CAD model. Before the next layer is added the viscous paste must turn to a solid structure (e.g. by a shear thinning and drying) to bear the weight of the next layers. This happens due to shear thinning property of the slurry. This technique usually does not need support structure. Materials with different properties can be printed by using 2 nozzles. Limitations are large building time, and only limited geometry [104].

Table 3. An overview of resolution of selected methods [104].

method	Layer thickness (μm)	Smallest feature (μm)
3DP	20–100	350–500
SLS	76 –100	45–100
RC	225–750	Rod diameter 200–400
FDM	250–370	Rod diameter 260–700
SLA	1–40	1–70

5. IMAGE ANALYSIS OF BONE TISSUE

The architecture of native bone tissue was studied on the mouse skeleton. The micro- and macroporosity has been evaluated in this chapter.

5.1. Methodology

For skeletal preparation, the bone samples were dissected from mouse cadavers and cleared by 3 M KOH for 4 days. After washing with distilled water, the bones were dehydrated with 80 % and 100 % ethanol followed by drying at 60 °C for 5 min.

Some parts of bone samples were broken with tweezer to disclose internal structures of bones and samples were oriented on aluminium stubs for gold sputtering using sputter SCD 040 (30 mA, 3 min, Balzers Union). Micrographs were acquired with scanning electron microscope Vega Tescan (Czech Republic). The pore and strut sizes and overall porosity was determined by ImageJ software (NIH, US).

Bones were isolated from mouse cadavers remaining from animal experiments approved by the Ministry of Education, Youth, and Sport of the Czech Republic under project number MSMT-15876/2013-310; supervised by the local ethical committee of the Faculty of Medicine, Masaryk University; and performed by certified individuals of the Department of Histology and Embryology.

5.2. Results

Examples of the microstructure of the bone tissue taken from different parts of the mouse skeleton are displayed in Fig. 14, Fig. 15, Fig. 16, and Fig. 17. It is evident that bone has different internal architecture depending on the bone location. The structure visible in the micrographs is consistent with the structure of bone at macroscale level described in the chapter 1.2. Thick compact layer was distinguishable on the outer surfaces of all bones, whereas the macroporous cancellous structure was found only inside the flat and short bones and in the epiphysis of long bones. Since this thesis is focused on porous synthetic bone grafts, bones without macropores are not shown here and further discussed.

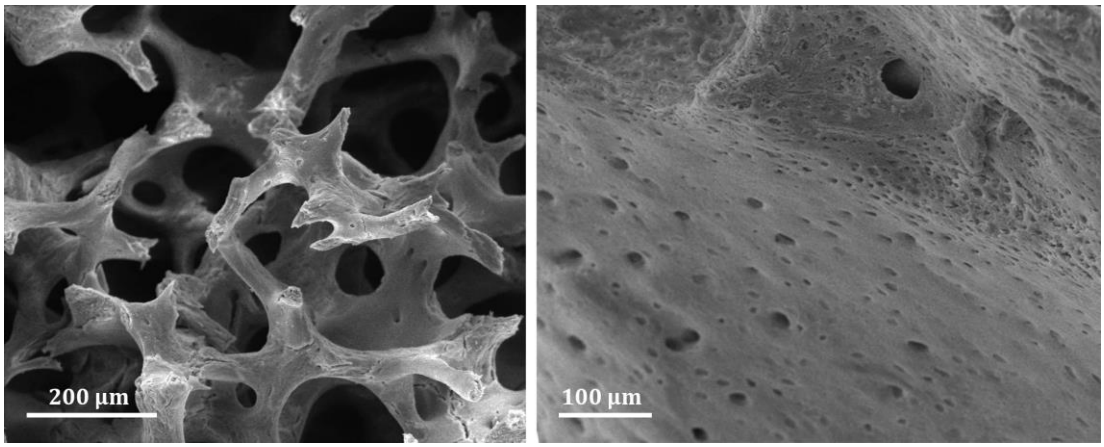

Fig. 14. Detail of macroporous trabecular structure and micropores in the cortical bone.

The observed bone tissue exhibited few types of pores which could be simply described as macro and micro pores (see Fig. 14). Macropore diameters varied between 20 and 200 μm and micropore size was 8.5 ± 3 μm. SEM observations further showed that bone structure was anisotropic; many pores, were elongated, probably in the direction of the applied load. This phenomena was visible mainly on epiphysis of long bones. The microstructure of samples exhibited significant differences between the sites, the morphology of trabeculae varied from rod-like to plate-like structure.

The dimensions of pores and trabeculae depicted in the Fig. 15 and Fig. 16 are summarized in the Table 4. The average (N=20) pore diameter was above 100 μm, which is in agreement with the minimum pore size recommended for synthetic bone grafts [61].

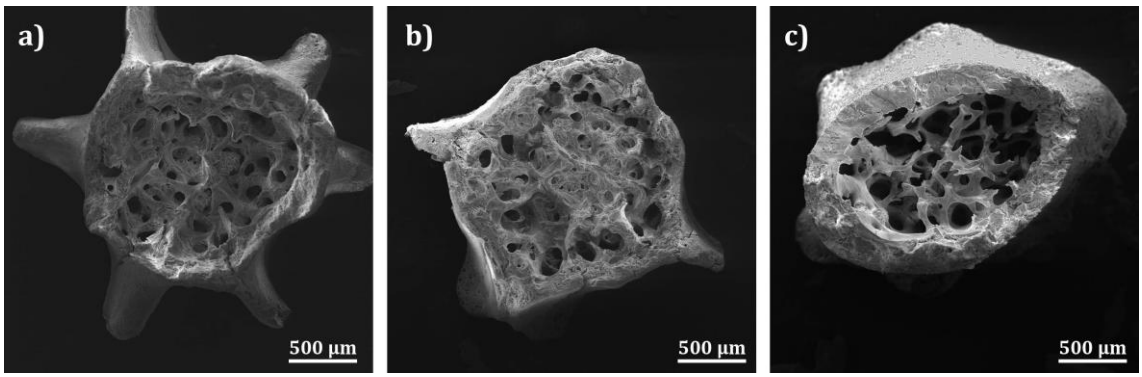

Fig. 15. Fractured cancellous bone tissues. (a) lumbar and (b) tail vertebrae and (c) femur epiphysis.

Table 4. Dimensional characteristics of selected bones.

Bone	Pore diameter (μm)	Strut thickness (μm)	Compact bone thickness (μm)
Vertebra (a)	101 ± 45	67 ± 19	209 ± 42
Vertebra (b)	145 ± 42	51 ± 17	137 ± 22
Femur	140 ± 54	40 ±14	235 ± 22
Pelvis	146 ± 32	43 ±14	–

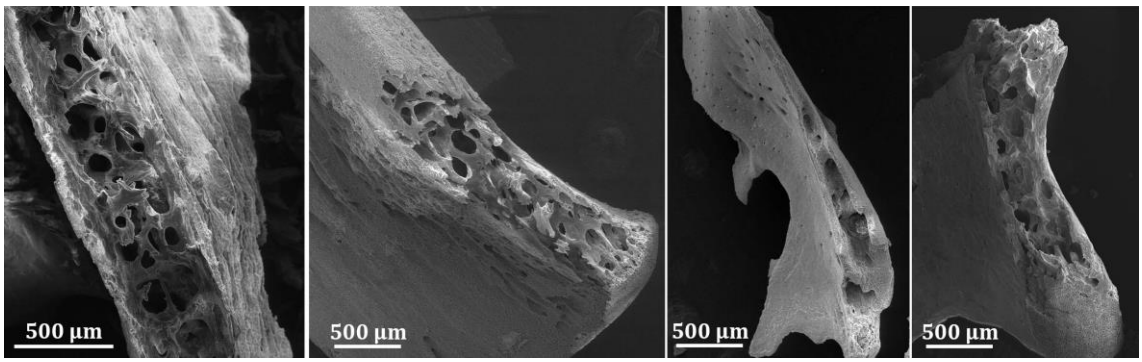

Fig. 16. Structure of flat bones. Pelvis – left images, shoulder blade – right images.

Fig. 17 shows a structure of an ethmoid bone and corresponding pore size distribution. For simplification, the pores were considered being circular; then the pore diameters were calculated from the measured pore area. It is evident that pores are smaller than pores in cancellous bones. The micropores below 10 μm were not evaluated here.

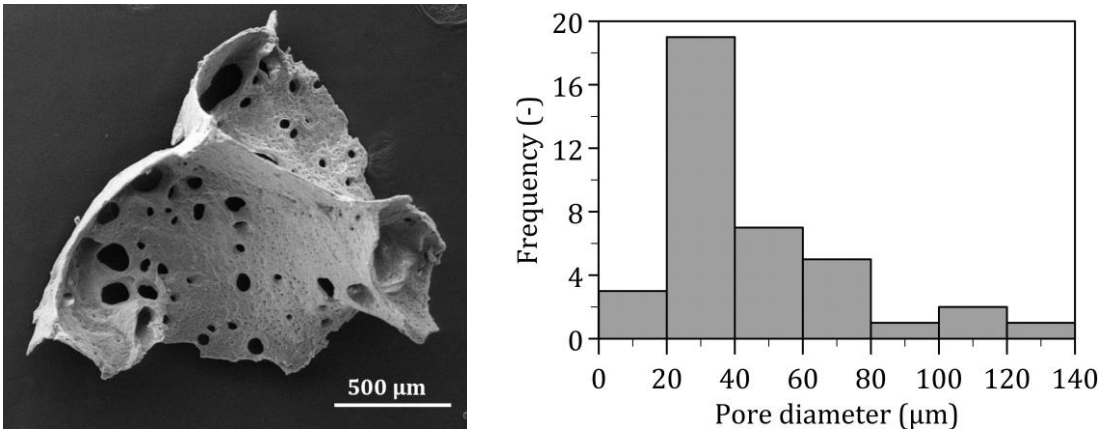

Fig. 17. Micrograph of os ethmoidale and the corresponding pore size distribution.

The estimated pore diameters have only indicative character because it is not possible to accurately describe a 3D structure from 2D images acquired in only one direction. The most accurate results would be obtained from μCT 3D analysis, including total porosity. However preparation and analysis with such technique is out of range of this thesis.

The measured thickness of trabeculae (~50μm) were in agreement with dimensions determined by μCT on rodents (20 – 60 μm) [106]. The comparison of our results with values referred for human bone tissue have been surprisingly quite similar [34]. The reported human trabecula thickness varied between 82 to 284 μm [107]. The macropore size (trabecular separation) of human cancellous bone was reported between 450 and 1310 μm [107]. Even though the trabeculae and pores of human bone are larger, the difference is almost negligible if we consider total dimensions of man and mouse. The difference is mostly in the overall volume of specific tissue which is determined by the size of species, but the microporosity is the same and trabecula size are quite similar. This could be related to the similar size of cells as structural elements.

6. CAD MODELING OF 3D SCAFFOLDS

Several scaffold models having various pore size and curvature were designed following the general bone scaffold requirements and according to the literature [87]. The external shape of the scaffolds, presented in this bachelor thesis, was designed with respect to the summarized parameters and our biological analysis. The overall external shape consisted of a disk (7.5 mm in diameter and 1.5 mm high) and four abutments (1 mm). The abutments were designed to potentially offset the scaffold from the bottom of the culture well during the testing and in a similar manner, to avoid a direct contact between the porous disk and the building platform of the stereolithography to preserve open macroporous structure of the printed scaffold. Initially, the abutments had been designed not to interfere with the disk geometry, however, the preliminary experiments revealed only limited cohesion (due to the small contact area) between abutments and scaffold, therefore the design was changed and the abutments were enlarged to penetrate to the outer scaffold surface.

As is depict in Fig. 18, four internal architectures with convex, flat, and concave curvatures were designed. Despite the different internal architecture all scaffolds were designed to have a constant porosity of 70 vol. % before the sintering. All structures were based on periodically repeated cubic elements, symmetrical in 3 directions. The first structure, composed of the cylindrical rods, was similar to structure obtained by robocasting, the resulting pores were thus convex. The second structure was formed by quadrangular prisms exhibiting a zero curvature. The third model was inverse to the first one; the 3D perpendicular cylinders were subtracting from the solid cube resulted in concave voids. The last structure was composed of interconnected circular pores.

Scaffolds of each architecture were designed to have three different pore sizes. Because it is quite tricky to determine the exact pore size due to the complex pore architecture, the dimensions of the cubic units were set, reaching approximately 450, 750 and 1100 μm. The corresponding pores than ranging from 240 μm (interconnections of the circular pores) to 1270 μm (diameter of the whole circular pore). The individual pore sizes are summarized in the Table 5.

Table 5. An overview of pore sizes of individual scaffold architectures. (Dimensions were measured at the surfaces of the modelled elementary cubic units; *a* is the square pore side, ⌀ is the circle diameter at the surface / diameter of the whole circular pore inside).

Cylindrical profiles	Quadrangular prisms	Cylindrical pores	Circular pores
a = 291	a = 307	⌀ 321	⌀ 243 / ⌀ 543
a = 419	a = 522	⌀ 587	⌀ 409 / ⌀ 904
a = 680	a = 720	⌀ 820	⌀ 571 / ⌀ 1267

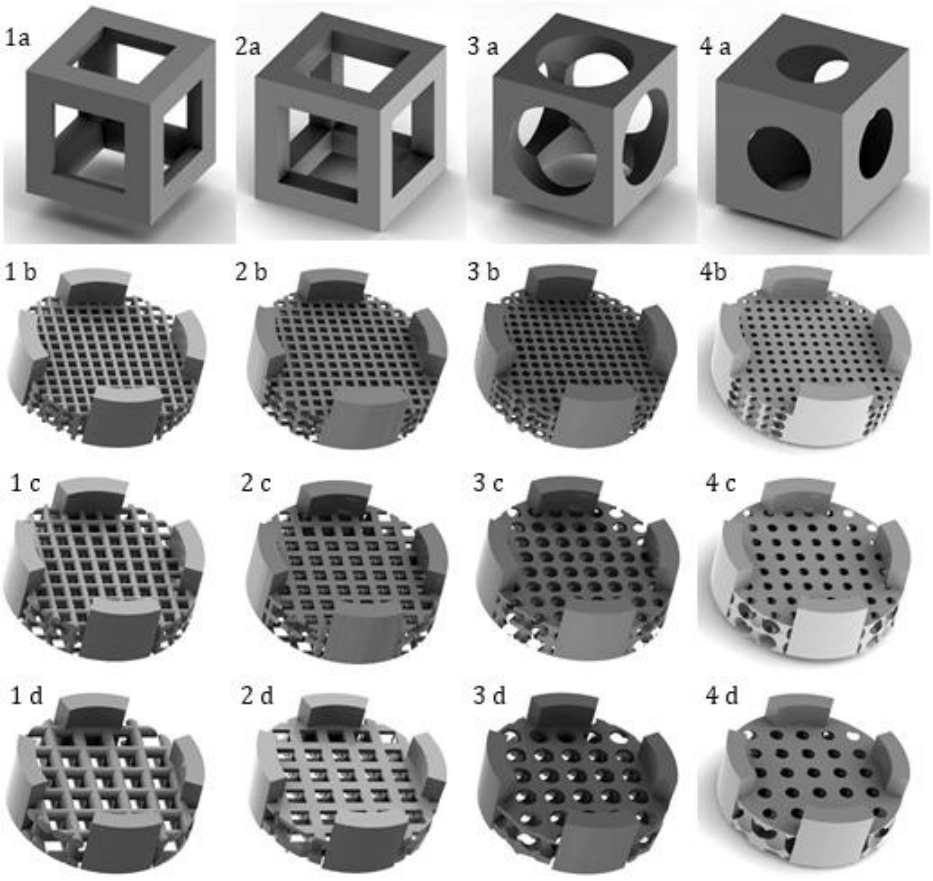

Fig. 18. Scaffolds designed to have different internal structure consisted of: (1) cylindrical rods, (2) quadrangular prisms, (3) cylindrical pores, (4) circular pores. Elementary cubic size is equal to: (b) 450 μm, (c) 750 μm, (b) 1100 μm.

Besides the structures based on the elemental cubic lattices, one more complex structure was modelled. As seen in Fig. 19, this structure consisted of 4 subunits, each of them composed of rods lying on the half of the body diagonal of the cube. This structure is called diamond cubic structure as diamond crystalizes in this lattice (carbon atoms are located at the intersections). The advantages of this lattice should be higher mechanical properties and better permeability, however, the individual rods are convex which might not be so beneficial for cell response. As in the previous case, the model was designed to fill space up to 30 vol. %. Structures were modelled having different pore sizes (330, 400, 540, and 890 μm).

Fig. 19. Diamond cubic structure: (a) elemental diamond structure, (b)-(e) scaffolds with diamond structure sorted with the increasing pore size.

7. STEREOLITHOGRAPHY OF CAD MODELS

The modelled scaffolds were manufactured by the Lithography based Ceramic Manufacturing (LCM) Technology. The LCM technology is based on the principle of photopolymerization. Ceramic powder is homogeneously dispersed in a light sensitive organic matrix and selectively structured through mask exposure. The body of stereolithograph system used for the experiments have consisted of a vat, filled with a photocurable dispersion. Through the rotation of the vat, a layer of dispersion has been applied with a static wiper blade. The vat has been transparent so that the slurry could be lit from below by LEDs. The projected image has been generated via a digital mirror device, consisted of more than two million individually operated mirrors, which have been illuminated by the LEDs.

7.1. Materials and methods

The scaffolds were printed by the stereolithograph CeraFab 7500 (Lithoz, Austria) using the commercial calcium phosphate based dispersion LithaBone TCP 200 (Lithoz, Austria). The exact composition is unknown, however, according to the data sheet, it should contain 50 – 100 % β–TCP and 5 – 10% multifunctional acrylate.

The CAD models designed in the Chapter 6 were exported to the binary .stl (STereoLithography) files which were then uploaded into the CeraFab DC software. Due to the very fine structure of the scaffolds, the slice thickness was set to the minimal possible value of 25 μm (the lateral resolution of the machine is 40 μm). After the finding the optimal processing parameters (especially exposure time and intensity), the structures were build layer by layer. The processing procedure is shown in the Fig. 20.

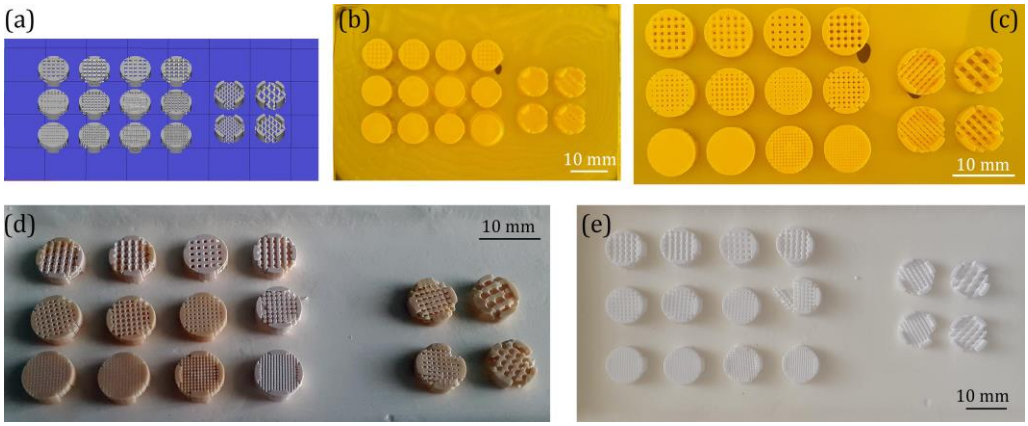

Fig. 20. Processing steps of scaffolds printed by stereolithography. (a) Samples layout in Lithoz DC software before printing; (b) freshly printed samples attached to the building platform with a dispersion residue; (c) samples after removing the surplus dispersion via compressed air; (d) samples after the final cleaning; (e) scaffolds sintered at 1100°C/3h.

The next step that followed the printing was the removal of the residual unpolymerised dispersion. The pore dimensions did not allow to remove the viscous dispersion from the internal structure just by compressed air, so the samples (still attached to the building platform were rinsed by the LithaSol 20

solvent (Lithoz, Austria). The solvent rinsing and compressed air blowing was repeated several times. Thereafter, the samples were removed from the platform and separately cleaned in the solvent. To increase the removal efficiency, the ultrasound was applied. This procedure (soaking / rinsing / blowing) was repeated until the unpolymerized dispersion had been completely removed.

The green bodies (here cleaned unsintered ceramic/photopolymer composites) were finally sintered in air at 1100 °C for 6 hours (Fig. 20e). According to the manufacturer's recommendations, the binder extraction should be very slow to avoid the collapse of the structure before being sintered; overall it took several days. The heat treatment protocol was slightly changed, it consisted of heating rate 0.5 °C/min up to 430 °C, three-hour-dwell, heating rate 0.7 °C/min up to 850 °C, one hour dwell, final heating rate 1 °C/min to 1100°C, 6-hour-dwell and 1 °C/min cooling rate to 250 °C.

The scaffold structure was characterised before and after the sintering by digital microscope DinoLite AM4115. Microstructure of the sintered scaffolds were also evaluated using scanning electron microscope Lyra (Tescan, Czech Republic).

7.2. Results and discussion

All designed scaffolds were successfully printed. The macrostructure of the sintered scaffolds with various internal architecture and three different pore sizes are shown in Fig. 21.

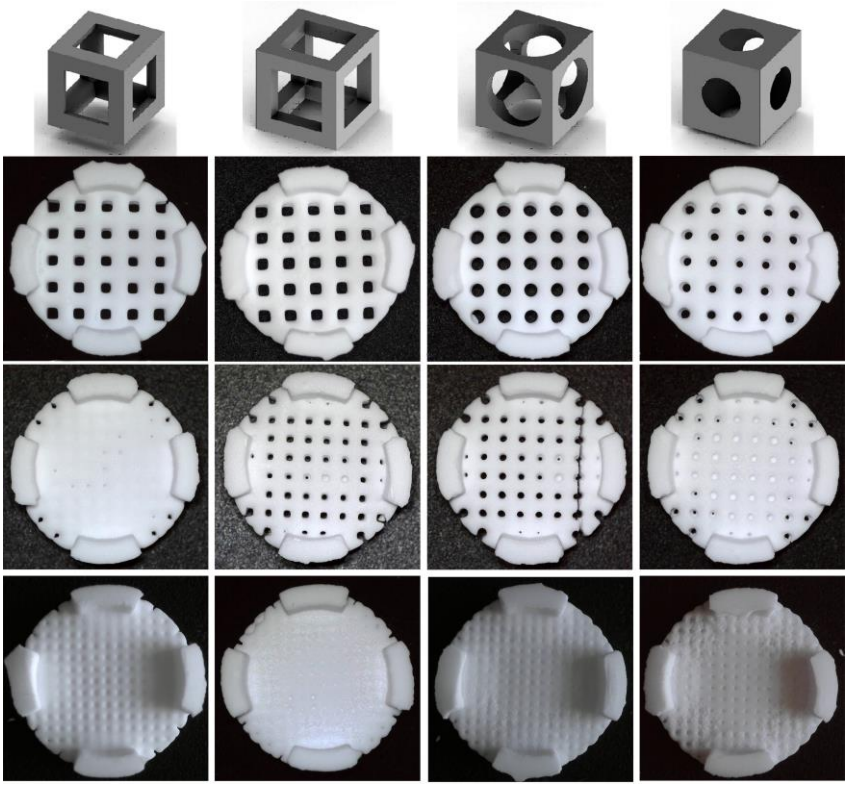

Fig. 21. Sintered scaffold macrostructures having different geometry. (The disk diameter is 7.5 mm).

Macroscopically, the shape of printed samples corresponded to the modelled design. However, the disks were bent in the central part, probably because they were not enough strong to withstand their own weight and the weight of the next layers during the printing when the first layer was attached only to the disk periphery. The visual observation showed that scaffolds with the largest pores were almost ideally replicated. The removal of unpolymerised dispersion from medium sized porous samples was not entirely successful as is evident from few sealed pores in the middle of the samples. The smallest pores seemed to be mostly filled.

One of the samples with cylindrical pores split during the processing and, overall, samples with this geometry were susceptible to the mechanical damage during the cleaning. Their elementary cubic unit is mechanically least convenient because the struts are locally the thinnest compared to other designs.

The pore geometry of the printed samples at higher magnification is shown in Fig. 22. It seems that shape and dimensions of printed and sintered pores slightly differ from the model. The originally square pores and prisms tend to be rounded – this phenomena is more evident with a decreasing pore size. The second difference compared to the original model lies in the pore size reduction. Generally, the pore sizes have been smaller than it was expected. For example, the largest square pores, designed to reach 720 μm, did not exceed 500 μm.

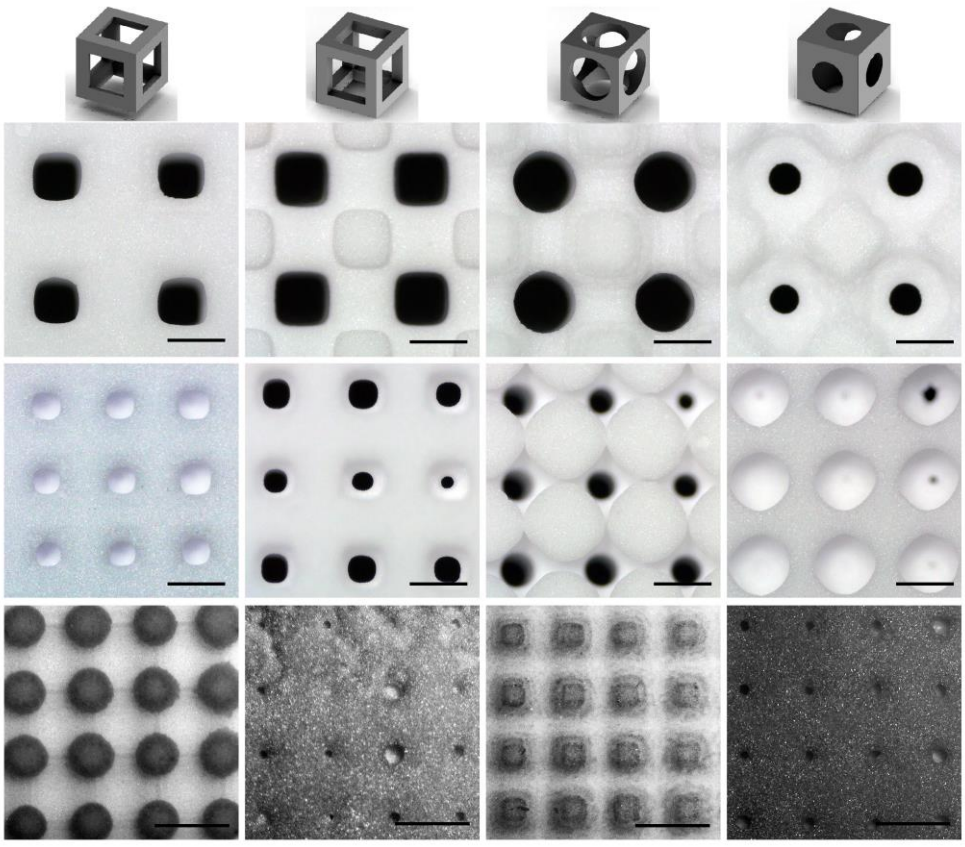

Fig. 22. The detailed view of the macrostructure of printed scaffolds. Scale bar 0.5 mm.

The shape and dimensions of the medium-size pores were also determined by

analysis of the SEM micrographs. The analysis confirmed that the pore size and geometry drastically changed. There was an approximately 50% drop in pore dimensions compared to the CAD models. Pores within cylindrical profiles decreased to 125 μm, quadrangular and circular pores reached 285 μm, and circular pores did not exceed 217 μm on the surface interconnection. The smallest sized pores (not shown here) were not larger than 100 μm.

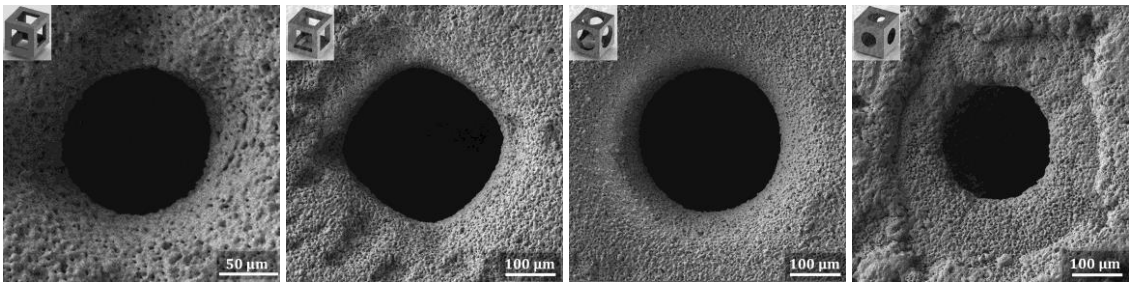

Fig. 23. Micrographs of middle-sized pores of various geometry.

As it was discussed in the previous chapters, bones and ideal scaffolds contain also micropores in addition to macropores. SEM analysis revealed about 10 vol. % porosity. Micropores were regularly arranged in the whole volume of the scaffolds. Micropores were open and interconnected with an average pore size 2.5 μm.

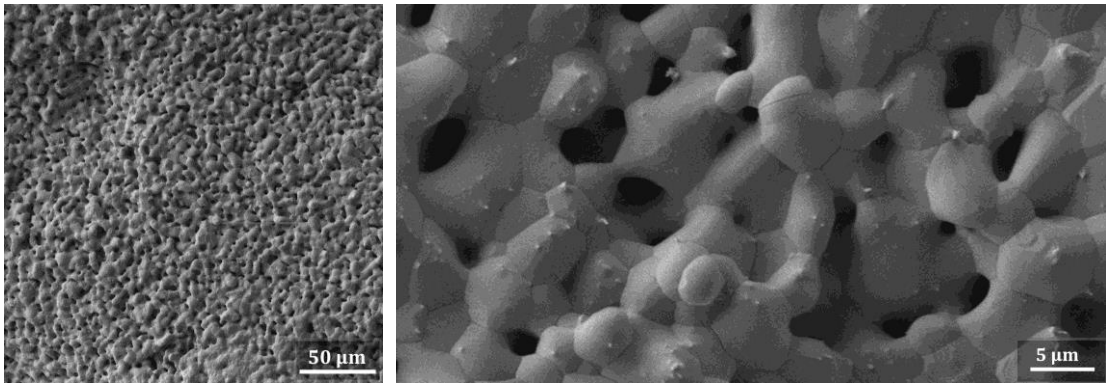

Fig. 24. Scaffold microstructure at different magnifications. The microporosity reached 10 vol. %. The average pore diameter was 2.5 μm.

Note: scaffolds with a diamond structure were also successfully printed, however, their macrostructure was destroyed when abrading the solid bottom supported layer.

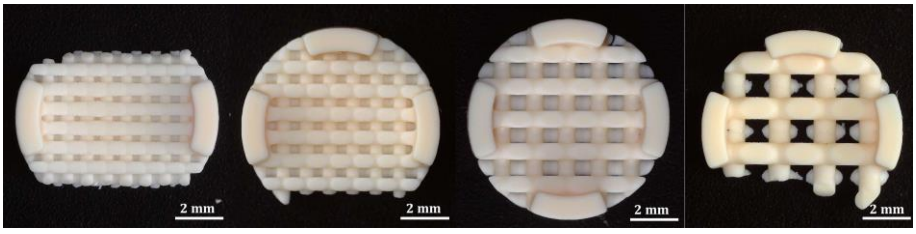

Fig. 25. Examples of printed scaffolds with diamond structure.

8. CONCLUSION

An extensive literature search dealing with structure of bone and synthetic bone replacements was performed. The bone scaffold requirements can be summarized as follows: material must be bioactive (e.g. calcium phosphate), the internal structure must be porous containing both macro and micro pores which both have to be interconnected, the surface curvature should ideally be concave. In the literature, there is no uniform conclusion about one ideal macropore size, so an image analysis of mouse skeleton was performed, showing that the macropores were about 50 to 200 μm large and micropores ranged between 5 and 12 μm. Bone arrangement was random, theoretically copying field lines which act locally.

Based on the above, CAD models were designed. Even though the structure of mouse bone is random, to simplify the model, the periodically repeated cubic units were designed. Four architectures varying in internal curvature were chosen: cylindrical profiles, quadrangular profiles, cylindrical and circular pores. Total porosity of models was 70%. The designed pore size, 240 to 1270 μm, was in accordance with a current state of the art. The size was higher than resulted from mouse bone analysis, because the proposed scaffolds are intended to be used in human medicine not in mice treatment.

The advantages and disadvantages of the individual preparation methods were discussed, finding that 3D printing is the most versatile technique. Hence, the CAD models were printed by the Lithography based Ceramic Manufacturing Technology using calcium-phosphate based dispersion. The printed scaffolds were macroscopically very precise, but the microstructure analysis revealed some problems. First of all, many of smaller pores were filled by unpolymerized dispersion causing the disappearing of macroporous structure after the sintering In future experiments it will be thus necessary to modify the process of dispersion removing, for example by applying high pressure or vacuum.

Anyway, scaffolds designed to have larger pores were nicely replicated with macropore sizes shifted to lower values, not exceeded 500 μm. The pores were interconnected both in macro and micro scale level. The micropores were about 3 μm large. The square pores tended to become rounded; it can be serious problem when studying dependence of surface curvature, nevertheless, with regard to medical use, it may even be beneficial, due to positive curvature and elimination of stress concentrators. To sum it up, from architectural point of view, printed scaffolds met all requirements placed on them; final pore size varying between 100 to 500 μm seemed to be optimal and moreover it was in accordance with results obtained on mouse bones. Objectives of the thesis were fulfilled. It was confirmed that scaffolds prepared by a stereolithography have a great potential for both research and bone tissue engineering applications.

LIST OF SYMBOLS AND ABBREVIATIONS

μCT	micro computed tomography
3D	three dimensional
ACP	amorphous calcium phosphates
AFM	atomic force microscopy
AM	additive manufacturing
Ca-P	calcium phosphate
CDHA	calcium-deficient hydroxyapatite
FDM	fused deposition modelling
HA	hydroxyapatite
LAB	laser assisted bioprinting
SEM	scanning electron microscopy
SFF	solid freeform fabrication
SLA	stereolithography
SLS	selective laser sintering
TCP	tricalcium phosphate

REFERENCES

[1] GIANNOUDIS, P. V., DINOPOULOS, H.,TSIRIDIS, E. Bone substitutes: An update, *Injury,* 2005, vol. 36, pp. S20.

[2] LANGER, R.,VACANTI, J. P. Tissue engineering, *Science (New York, N.Y.),* 1993, vol. 260, pp. 920.

[3] WOJNAR, R. In *Biomechanics of Hard Tissues*; Wiley-VCH Verlag GmbH & Co. KGaA: 2010, p 1.

[4] SHARIR, A., BARAK, M. M.,SHAHAR, R. Whole bone mechanics and mechanical testing, *The Veterinary Journal,* 2008, vol. 177, pp. 8.

[5] VAUGHAN, T. J., MCCARTHY, C. T.,MCNAMARA, L. M. A three-scale finite element investigation into the effects of tissue mineralisation and lamellar organisation in human cortical and trabecular bone, *Journal of the Mechanical Behavior of Biomedical Materials,* 2012, vol. 12, pp. 50.

[6] CLARKE, B. Normal Bone Anatomy and Physiology, *Clinical Journal of the American Society of Nephrology,* 2008, vol. 3, pp. S131.

[7] FLORENCIO-SILVA, R., SASSO, G. R., SASSO-CERRI, E., SIMOES, M. J.,CERRI, P. S. Biology of Bone Tissue: Structure, Function, and Factors That Influence Bone Cells, *Biomed Res Int,* 2015, vol. 2015, pp. 421746.

[8] OFTADEH, R., PEREZ-VILORIA, M., VILLA-CAMACHO, J. C., VAZIRI, A.,NAZARIAN, A. Biomechanics and Mechanobiology of Trabecular Bone: A Review, *Journal of Biomechanical Engineering,* 2015, vol. 137, pp. 0108021.

[9] MA, P. X.,ELISSEEFF, J. *Scaffolding In Tissue Engineering*; Taylor & Francis, 2005.

[10] REY, C., COMBES, C., DROUET, C.,GLIMCHER, M. J. Bone mineral: update on chemical composition and structure, *Osteoporosis International,* 2009, vol. 20, pp. 1013.

[11] RHO, J.-Y., KUHN-SPEARING, L.,ZIOUPOS, P. Mechanical properties and the hierarchical structure of bone, *Medical Engineering & Physics,* 1998, vol. 20, pp. 92.

[12] WOPENKA, B.,PASTERIS, J. D. A mineralogical perspective on the apatite in bone, *Materials Science and Engineering: C,* 2005, vol. 25, pp. 131.

[13] YOSHIKAWA, H.,MYOUI, A. Bone tissue engineering with porous hydroxyapatite ceramics, *J Artif Organs,* 2005, vol. 8, pp. 131.

[14] OLSZTA, M. J., CHENG, X., JEE, S. S., KUMAR, R., KIM, Y.-Y., KAUFMAN, M. J., DOUGLAS, E. P.,GOWER, L. B. Bone structure and formation: A new perspective, *Materials Science and Engineering: R: Reports,* 2007, vol. 58, pp. 77.

[15] WEINER, S.,WAGNER, H. D. THE MATERIAL BONE: Structure-Mechanical Function Relations, *Annual Review of Materials Science,* 1998, vol. 28, pp. 271.

[16] In *Nanoceramics in Clinical Use: From Materials to Applications (2)*; The Royal Society of Chemistry: 2016, p 1.

[17] FRANZ-ODENDAAL, T. A., HALL, B. K.,WITTEN, P. E. Buried alive: How osteoblasts become osteocytes, *Developmental Dynamics,* 2006, vol. 235, pp. 176.

[18] DALLAS, S. L., PRIDEAUX, M.,BONEWALD, L. F. The Osteocyte: An Endocrine Cell … and More, *Endocrine Reviews,* 2013, vol. 34, pp. 658.

[19] RUBIN, M. A.,JASIUK, I. The TEM characterization of the lamellar structure of osteoporotic human trabecular bone, *Micron,* 2005, vol. 36, pp. 653.

[20] RITCHIE, R. O. The conflicts between strength and toughness, *Nat Mater,*

2011, vol. 10, pp. 817.
[21] FRATZL, P.,WEINKAMER, R. Nature's hierarchical materials, *Progress in Materials Science,* 2007, vol. 52, pp. 1263.
[22] WEINER, S.,TRAUB, W. Bone structure: from angstroms to microns, *The FASEB Journal,* 1992, vol. 6, pp. 879.
[23] WEINER, S., TRAUB, W.,WAGNER, H. D. Lamellar Bone: Structure–Function Relations, *Journal of Structural Biology,* 1999, vol. 126, pp. 241.
[24] VAN OERS, R. F. M., RUIMERMAN, R., VAN RIETBERGEN, B., HILBERS, P. A. J.,HUISKES, R. Relating osteon diameter to strain, *Bone,* 2008, vol. 43, pp. 476.
[25] VANPUTTE, C., REGAN, J.,RUSSO, A. *Seeley's Essentials of Anatomy and Physiology*; McGraw-Hill Education, 2012.
[26] HAWKINS, D. In *Biomechanics of Musculoskeletal Tissues*; University of California: Davis, 2001, p 13.
[27] KEAVENY, T. M.,HAYES, W. C. Mechanical properties of cortical and trabecular bone, *Bone,* 1993, vol. 7, pp. 285.
[28] WANG, X., XU, S., ZHOU, S., XU, W., LEARY, M., CHOONG, P., QIAN, M., BRANDT, M.,XIE, Y. M. Topological design and additive manufacturing of porous metals for bone scaffolds and orthopaedic implants: A review, *Biomaterials,* 2016, vol. 83, pp. 127.
[29] CAMBRIDGE, U. O. *TLP Library Structure of bone and implant materials - Mechanical properties of bone* 2014 http://www.doitpoms.ac.uk/tlplib/bones/bone_mechanical.php.
[30] REZWAN, K., CHEN, Q. Z., BLAKER, J. J.,BOCCACCINI, A. R. Biodegradable and bioactive porous polymer/inorganic composite scaffolds for bone tissue engineering, *Biomaterials,* 2006, vol. 27, pp. 3413.
[31] FU, Q., SAIZ, E., RAHAMAN, M. N.,TOMSIA, A. P. Toward strong and tough glass and ceramic scaffolds for bone repair, *Advanced Functional Materials,* 2013, vol. 23, pp. 5461.
[32] RAVAGLIOLI, A.,KRAJEWSKI, A. *Bioceramics*; Springer Netherlands, 1992.
[33] LAUNEY, M. E., BUEHLER, M. J.,RITCHIE, R. O. On the mechanistic origins of toughness in bone, *Annual review of materials research,* 2010, vol. 40, pp. 25.
[34] KEAVENY, T. M., MORGAN, E. F., NIEBUR, G. L.,YEH, O. C. Biomechanics of trabecular bone, *Annual review of biomedical engineering,* 2001, vol. 3, pp. 307.
[35] RITCHIE, R. O., BUEHLER, M. J.,HANSMA, P. Plasticity and toughness in bone, *Phys. Today,* 2009, vol. 62, pp. 41.
[36] MARCUS, R., FELDMAN, D., DEMPSTER, D. W., LUCKEY, M.,CAULEY, J. A. *Osteoporosis: Two-Volume Set*; Elsevier Science, 2013.
[37] HENCH, L. L.,POLAK, J. M. Third-generation biomedical materials, *Science (New York, N.Y.),* 2002, vol. 295, pp. 1014.
[38] JONES, J. R.,BOCCACCINI, A. R. In *Cellular Ceramics*; Wiley-VCH Verlag GmbH & Co. KGaA: 2006, p 547.
[39] LU, J., FLAUTRE, B., ANSELME, K., HARDOUIN, P., GALLUR, A., DESCAMPS, M.,THIERRY, B. Role of interconnections in porous bioceramics on bone recolonization in vitro and in vivo, *Journal of Materials Science: Materials in Medicine,* 1999, vol. 10, pp. 111.
[40] LIU, Y., LIM, J.,TEOH, S. H. Review: development of clinically relevant scaffolds for vascularised bone tissue engineering, *Biotechnol Adv,* 2013, vol. 31,

pp. 688.
[41] HENCH, L. L. Sol-gel materials for bioceramic applications, *Current Opinion in Solid State and Materials Science,* 1997, vol. 2, pp. 604.
[42] HUTMACHER, D. W. Scaffolds in tissue engineering bone and cartilage, *Biomaterials,* 2000, vol. 21, pp. 2529.
[43] BOSE, S., ROY, M.,BANDYOPADHYAY, A. Recent advances in bone tissue engineering scaffolds, *Trends in biotechnology,* 2012, vol. 30, pp. 546.
[44] LICHTE, P., PAPE, H. C., PUFE, T., KOBBE, P.,FISCHER, H. Scaffolds for bone healing: Concepts, materials and evidence, *Injury,* 2011, vol. 42, pp. 569.
[45] KARAGEORGIOU, V.,KAPLAN, D. Porosity of 3D biomaterial scaffolds and osteogenesis, *Biomaterials,* 2005, vol. 26, pp. 5474.
[46] RAHAMAN, M. N., DAY, D. E., BAL, B. S., FU, Q., JUNG, S. B., BONEWALD, L. F.,TOMSIA, A. P. Bioactive glass in tissue engineering, *Acta biomaterialia,* 2011, vol. 7, pp. 2355.
[47] HENCH, L. L. Bioglass: 10 milestones from concept to commerce, *Journal of Non-Crystalline Solids,* 2016, vol. 432, Part A, pp. 2.
[48] MASTROGIACOMO, M., SCAGLIONE, S., MARTINETTI, R., DOLCINI, L., BELTRAME, F., CANCEDDA, R.,QUARTO, R. Role of scaffold internal structure on in vivo bone formation in macroporous calcium phosphate bioceramics, *Biomaterials,* 2006, vol. 27, pp. 3230.
[49] SONG, G., HABIBOVIC, P., BAO, C., HU, J., VAN BLITTERSWIJK, C. A., YUAN, H., CHEN, W.,XU, H. H. K. The homing of bone marrow MSCs to non-osseous sites for ectopic bone formation induced by osteoinductive calcium phosphate, *Biomaterials,* 2013, vol. 34, pp. 2167.
[50] SAMAVEDI, S., WHITTINGTON, A. R.,GOLDSTEIN, A. S. Calcium phosphate ceramics in bone tissue engineering: A review of properties and their influence on cell behavior, *Acta Biomaterialia,* 2013, vol. 9, pp. 8037.
[51] BOHNER, M. Resorbable biomaterials as bone graft substitutes, *Materials Today,* 2010, vol. 13, pp. 24.
[52] DOROZHKIN, S. V. Calcium orthophosphates: Occurrence, properties, biomineralization, pathological calcification and biomimetic applications, *Biomatter,* 2011, vol. 1, pp. 121.
[53] CARRODEGUAS, R. G.,DE AZA, S. α-Tricalcium phosphate: Synthesis, properties and biomedical applications, *Acta Biomaterialia,* 2011, vol. 7, pp. 3536.
[54] KLEIN, C. P. A. T., DE BLIECK-HOGEMRST, J. M. A., WOLKET, J. G. C.,DE GROOT, K. Studies of the solubility of different calcium phosphate ceramic particles in vitro, *Biomaterials,* 1990, vol. 11, pp. 509.
[55] BOHNER, M.,LEMAITRE, J. Can bioactivity be tested in vitro with SBF solution?, *Biomaterials,* 2009, vol. 30, pp. 2175.
[56] NILEN, R. W.,RICHTER, P. W. The thermal stability of hydroxyapatite in biphasic calcium phosphate ceramics, *Journal of materials science. Materials in medicine,* 2008, vol. 19, pp. 1693.
[57] JARCHO, M. Calcium Phosphate Ceramics as Hard Tissue Prosthetics, *Clinical Orthopaedics and Related Research,* 1981, vol. 157, pp. 259.
[58] DURUCAN, C.,BROWN, P. W. Kinetic Model for α–Tricalcium Phosphate Hydrolysis, *Journal of the American Ceramic Society,* 2002, vol. 85, pp. 2013.
[59] VANI, R., GIRIJA, E. K., ELAYARAJA, K., PRAKASH PARTHIBAN, S.,

KESAVAMOORTHY, R.,NARAYANA KALKURA, S. Hydrothermal synthesis of porous triphasic hydroxyapatite/(alpha and beta) tricalcium phosphate, *Journal of materials science. Materials in medicine,* 2009, vol. 20 Suppl 1, pp. S43.
[60] PEREZ, R. A.,MESTRES, G. Role of pore size and morphology in musculo-skeletal tissue regeneration, *Materials science & engineering. C, Materials for biological applications,* 2016, vol. 61, pp. 922.
[61] KARAGEORGIOU, V.,KAPLAN, D. Porosity of 3D biomaterial scaffolds and osteogenesis, *Biomaterials,* 2005, vol. 26, pp. 5474.
[62] HING, K. A., ANNAZ, B., SAEED, S., REVELL, P. A.,BUCKLAND, T. Microporosity enhances bioactivity of synthetic bone graft substitutes, *Journal of Materials Science: Materials in Medicine,* 2005, vol. 16, pp. 467.
[63] GARIBOLDI, M. I.,BEST, S. M. Effect of Ceramic Scaffold Architectural Parameters on Biological Response, *Frontiers in Bioengineering and Biotechnology,* 2015, vol. 3, pp. 151.
[64] HABIBOVIC, P., YUAN, H., VAN DER VALK, C. M., MEIJER, G., VAN BLITTERSWIJK, C. A.,DE GROOT, K. 3D microenvironment as essential element for osteoinduction by biomaterials, *Biomaterials,* 2005, vol. 26, pp. 3565.
[65] HING, K. A. Bioceramic Bone Graft Substitutes: Influence of Porosity and Chemistry, *International Journal of Applied Ceramic Technology,* 2005, vol. 2, pp. 184.
[66] MALMSTRÖM, J., ADOLFSSON, E., ARVIDSSON, A.,THOMSEN, P. Bone Response Inside Free-Form Fabricated Macroporous Hydroxyapatite Scaffolds with and without an Open Microporosity, *Clinical Implant Dentistry and Related Research,* 2007, vol. 9, pp. 79.
[67] BIGNON, A., CHOUTEAU, J., CHEVALIER, J., FANTOZZI, G., CARRET, J. P., CHAVASSIEUX, P., BOIVIN, G., MELIN, M.,HARTMANN, D. Effect of micro- and macroporosity of bone substitutes on their mechanical properties and cellular response, *Journal of Materials Science: Materials in Medicine,* 2003, vol. 14, pp. 1089.
[68] BARRADAS, A. M., YUAN, H., VAN BLITTERSWIJK, C. A.,HABIBOVIC, P. Osteoinductive biomaterials: current knowledge of properties, experimental models and biological mechanisms, *European cells & materials,* 2011, vol. 21, pp. 407.
[69] ZHANG, J., BARBIERI, D., TEN HOOPEN, H., DE BRUIJN, J. D., VAN BLITTERSWIJK, C. A.,YUAN, H. Microporous calcium phosphate ceramics driving osteogenesis through surface architecture, *Journal of Biomedical Materials Research Part A,* 2015, vol. 103, pp. 1188.
[70] ROUAHI, M., GALLET, O., CHAMPION, E., DENTZER, J., HARDOUIN, P.,ANSELME, K. Influence of hydroxyapatite microstructure on human bone cell response, *Journal of Biomedical Materials Research Part A,* 2006, vol. 78A, pp. 222.
[71] RECHENDORFF, K., HOVGAARD, M. B., FOSS, M., ZHDANOV, V. P.,BESENBACHER, F. Enhancement of Protein Adsorption Induced by Surface Roughness, *Langmuir,* 2006, vol. 22, pp. 10885.
[72] HULBERT, S. F., YOUNG, F. A., MATHEWS, R. S., KLAWITTER, J. J., TALBERT, C. D.,STELLING, F. H. Potential of ceramic materials as permanently implantable skeletal prostheses, *Journal of Biomedical Materials Research,* 1970, vol. 4, pp. 433.
[73] KLAWITTER, J. J.,HULBERT, S. F. Application of porous ceramics for the

attachment of load bearing internal orthopedic applications, *Journal of Biomedical Materials Research,* 1971, vol. 5, pp. 161.
[74] JOLY, P., DUDA, G. N., SCHONE, M., WELZEL, P. B., FREUDENBERG, U., WERNER, C.,PETERSEN, A. Geometry-driven cell organization determines tissue growths in scaffold pores: consequences for fibronectin organization, *PLoS One,* 2013, vol. 8, pp. e73545.
[75] FENG, B., JINKANG, Z., ZHEN, W., JIANXI, L., JIANG, C., JIAN, L., GUOLIN, M.,XIN, D. The effect of pore size on tissue ingrowth and neovascularization in porous bioceramics of controlled architecture in vivo, *Biomed Mater,* 2011, vol. 6, pp. 015007.
[76] ZADPOOR, A. A. Bone tissue regeneration: the role of scaffold geometry, *Biomater Sci,* 2015, vol. 3, pp. 231.
[77] BIDAN, C. M., KOMMAREDDY, K. P., RUMPLER, M., KOLLMANNSBERGER, P., BRECHET, Y. J. M., FRATZL, P.,DUNLOP, J. W. C. How Linear Tension Converts to Curvature: Geometric Control of Bone Tissue Growth, *Plos One,* 2012, vol. 7, pp.
[78] BIDAN, C. M., WANG, F. M.,DUNLOP, J. W. A three-dimensional model for tissue deposition on complex surfaces, *Comput Method Biomec,* 2013, vol. 16, pp. 1056.
[79] GAMSJAGER, E., BIDAN, C. M., FISCHER, F. D., FRATZL, P.,DUNLOP, J. W. C. Modelling the role of surface stress on the kinetics of tissue growth in confined geometries, *Acta Biomaterialia,* 2013, vol. 9, pp. 5531.
[80] RUMPLER, M., WOESZ, A., DUNLOP, J. W. C., VAN DONGEN, J. T.,FRATZL, P. The effect of geometry on three-dimensional tissue growth, *Journal of the Royal Society Interface,* 2008, vol. 5, pp. 1173.
[81] SCARANO, A., PERROTTI, V., ARTESE, L., DEGIDI, M., DEGIDI, D., PIATTELLI, A.,IEZZI, G. Blood vessels are concentrated within the implant surface concavities: a histologic study in rabbit tibia, *Odontology,* 2014, vol. 102, pp. 259.
[82] MELCHELS, F. P., BARRADAS, A. M., VAN BLITTERSWIJK, C. A., DE BOER, J., FEIJEN, J.,GRIJPMA, D. W. Effects of the architecture of tissue engineering scaffolds on cell seeding and culturing, *Acta Biomater,* 2010, vol. 6, pp. 4208.
[83] LU, J. X., FLAUTRE, B., ANSELME, K., HARDOUIN, P., GALLUR, A., DESCAMPS, M.,THIERRY, B. Role of interconnections in porous bioceramics on bone recolonization in vitro and in vivo, *Journal of materials science. Materials in medicine,* 1999, vol. 10, pp. 111.
[84] SOBRAL, J. M., CARIDADE, S. G., SOUSA, R. A., MANO, J. F.,REIS, R. L. Three-dimensional plotted scaffolds with controlled pore size gradients: Effect of scaffold geometry on mechanical performance and cell seeding efficiency, *Acta Biomaterialia,* 2011, vol. 7, pp. 1009.
[85] ZHANG, X.-Y., FANG, G.,ZHOU, J. Additively Manufactured Scaffolds for Bone Tissue Engineering and the Prediction of their Mechanical Behavior: A Review, *Materials,* 2017, vol. 10, pp. 50.
[86] CHEAH, C. M., CHUA, C. K., LEONG, K. F.,CHUA, S. W. Development of a Tissue Engineering Scaffold Structure Library for Rapid Prototyping. Part 1: Investigation and Classification, *The International Journal of Advanced Manufacturing Technology,* 2003, vol. 21, pp. 291.
[87] KOLAN, K. C., LEU, M. C., HILMAS, G.,COMTE, T. In *Proceedings of the 24th Annual International Solid Freeform Fabrication Symposium*; Austin: 2013, p 816.

[88] OHJI, T.,FUKUSHIMA, M. Macro-porous ceramics: processing and properties, *International Materials Reviews,* 2012, vol. 57, pp. 115.
[89] JEAN, G., SCIAMANNA, V., DEMUYNCK, M., CAMBIER, F.,GONON, M. Macroporous ceramics: Novel route using partial sintering of alumina-powder agglomerates obtained by spray-drying, *Ceramics International,* 2014, vol., pp.
[90] STUDART, A. R., GONZENBACH, U. T., TERVOORT, E.,GAUCKLER, L. J. Processing Routes to Macroporous Ceramics: A Review, *Journal of the American Ceramic Society,* 2006, vol. 89, pp. 1771.
[91] KARL, S.,SOMERS, A. V.; Google Patents: 1963.
[92] COLOMBO, P. Conventional and novel processing methods for cellular ceramics, *Philosophical Transactions of the Royal Society A: Mathematical, Physical and Engineering Sciences,* 2006, vol. 364, pp. 109.
[93] FU, Q., RAHAMAN, M. N., DOGAN, F.,BAL, B. S. Freeze casting of porous hydroxyapatite scaffolds. I. Processing and general microstructure, *Journal of Biomedical Materials Research Part B: Applied Biomaterials,* 2008, vol. 86B, pp. 125.
[94] DEVILLE, S., SAIZ, E.,TOMSIA, A. P. Freeze casting of hydroxyapatite scaffolds for bone tissue engineering, *Biomaterials,* 2006, vol. 27, pp. 5480.
[95] WEGST, U. G., SCHECTER, M., DONIUS, A. E.,HUNGER, P. M. Biomaterials by freeze casting, *Philos Trans A Math Phys Eng Sci,* 2010, vol. 368, pp. 2099.
[96] MACCHETTA, A., TURNER, I. G.,BOWEN, C. R. Fabrication of HA/TCP scaffolds with a graded and porous structure using a camphene-based freeze-casting method, *Acta Biomaterialia,* 2009, vol. 5, pp. 1319.
[97] DEVILLE, S. Freeze-Casting of Porous Biomaterials: Structure, Properties and Opportunities, *Materials,* 2010, vol. 3, pp. 1913.
[98] JONES, J. R.,HENCH, L. L. Regeneration of trabecular bone using porous ceramics, *Current Opinion in Solid State and Materials Science,* 2003, vol. 7, pp. 301.
[99] BARG, S., SOLTMANN, C., ANDRADE, M., KOCH, D.,GRATHWOHL, G. Cellular Ceramics by Direct Foaming of Emulsified Ceramic Powder Suspensions, *Journal of the American Ceramic Society,* 2008, vol. 91, pp. 2823.
[100] TRUNEC, M.,MACA, K. In *Advanced Ceramics for Dentistry*; SHEN, J. Z., KOSMAČ, T., Eds.; Butterworth-Heinemann: Oxford, 2014, p 123.
[101] THAVORNYUTIKARN, B., CHANTARAPANICH, N., SITTHISERIPRATIP, K., THOUAS, G. A.,CHEN, Q. Bone tissue engineering scaffolding: computer-aided scaffolding techniques, *Progress in Biomaterials,* 2014, vol. 3, pp. 61.
[102] BRUNELLO, G., SIVOLELLA, S., MENEGHELLO, R., FERRONI, L., GARDIN, C., PIATTELLI, A., ZAVAN, B.,BRESSAN, E. Powder-based 3D printing for bone tissue engineering, *Biotechnology Advances,* 2016, vol. 34, pp. 740.
[103] FIELDING, G. A., BANDYOPADHYAY, A.,BOSE, S. Effects of silica and zinc oxide doping on mechanical and biological properties of 3D printed tricalcium phosphate tissue engineering scaffolds, *Dental Materials,* 2012, vol. 28, pp. 113.
[104] BUTSCHER, A., BOHNER, M., HOFMANN, S., GAUCKLER, L.,MULLER, R. Structural and material approaches to bone tissue engineering in powder-based three-dimensional printing, *Acta Biomaterialia,* 2011, vol. 7, pp. 907.
[105] MELCHELS, F. P. W., FEIJEN, J.,GRIJPMA, D. W. A review on stereolithography and its applications in biomedical engineering, *Biomaterials,* 2010, vol. 31, pp. 6121.
[106] BOUXSEIN, M. L., BOYD, S. K., CHRISTIANSEN, B. A., GULDBERG, R. E.,

JEPSEN, K. J.,MULLER, R. Guidelines for assessment of bone microstructure in rodents using micro-computed tomography, *Journal of bone and mineral research : the official journal of the American Society for Bone and Mineral Research,* 2010, vol. 25, pp. 1468.
[107] HILDEBRAND, T., LAIB, A., MÜLLER, R., DEQUEKER, J.,RÜEGSEGGER, P. Direct Three-Dimensional Morphometric Analysis of Human Cancellous Bone: Microstructural Data from Spine, Femur, Iliac Crest, and Calcaneus, *Journal of Bone and Mineral Research,* 1999, vol. 14, pp. 1167.